Spring 5-2020

Design and Construction of a Computer Controlled Astronomical Spectropolarimeter

Jacob Marchio
University of Maine, jacob.marchio@maine.edu

DESIGN AND CONSTRUCTION OF A COMPUTER CONTROLLED ASTRONOMICAL SPECTROPOLARIMETER

by

Jacob Marchio

A Thesis Submitted for Partial Fulfillment
of the Requirements for a Degree with Honors
(Engineering Physics)

The Honors College

The University of Maine

May 2020

Advisory Committee
- Sam Hess, Professor of Physics, Advisor
- Francois Amar, Dean of The Honors College
- David Batuski, Professor of Physics
- Richard Eason, Associate Professor of Electrical and Computer Engineering
- Brian Frederick, Professor of Chemistry

ABSTRACT

A theoretical description of a simple optical train, modulated signal based spectropolarimeter is discussed. The design includes, after the telescope optical tube (in this case, a 9.25" Schmidt Cassegrain), a rotating quarter waveplate (compensator), a fixed linear polarizer (analyzer), and transmission grating of $100l/\text{mm}$, with a ZWO ASI290mm astronomical camera. The practical constraints on implementing such an instrument are discussed, and the construction of the spectropolarimeter is detailed, including the necessary optics, optomechanics, and electromechanics. The rotation and recording of the rotating compensator is facilitated by a motorized connection with proportional feedback control, and the uncertainty in measuring the angle is discussed. Calibration data from measurements with linear and circular polarizations was collected and analyzed, and exhibited close to the expected theoretical performance. Full analysis of the light in terms of the 4 Stoke's parameters was hindered by lack of knowledge of the relative angle between analyzer and compensator, leading to ambiguity in the S_1 and S_2 parameters; however, even with this ambiguity, degrees of polarization can be determined. Astronomical data was collected on the Moon, Arcturus, and Vega. The analyzed moonlight exhibited clear linear polarization, with a degree of polarization of 4.13%. The polarimetric analysis of Vega and Arcturus suggested potential for polarization, but more analysis is needed. Spectroscopic performance was confirmed by measuring the hydrogen Balmer lines in Vega, leading to a plate scale of $0.6434\frac{\text{nm}}{\text{px}}$. In summary, a low cost, low complexity spectropolarimeter capable of measuring all 4 Stoke's parameters of stellar spectra has been constructed and tested on known generated polarization signals and astronomical objects.

TABLE OF CONTENTS

LIST OF FIGURES

INTRODUCTION

In astronomy, gathering information about objects in space is made difficult by the vast scale and size of astronomical systems. Planets and asteroids are, perhaps, close enough to visit with spacecraft to study, but stars and nebulae are at this time too far to visit and galaxies are farther and larger still. Furthermore, the spatial extent of astronomical objects is limited in the sky, and for stars no true spatial detail is attainable with optical telescopes. All information about such object must be gathered from faint point sources of light. However, even light from point sources can contain information. Spectroscopy is a common form of analysis for astronomical objects. Through spectroscopy, the distribution of wavelengths contained in the starlight is analyzed. Taking stars as an approximation of black body radiators, the temperature, and therefore mass, of a star can be determined as well as atmospheric chemical composition through absorption and emission lines. There is more to light than just wavelengths: there is also the polarization. In astronomy, polarimetry is a less common form of analysis, but has been used to determine the existence of stellar dust envelopes, magnetic properties of stars [3], and is even used in analyzing supernovae [4].

THEORY

Light is described in electrodynamics to be an electromagnetic wave, described by the perpendicular simultaneous oscillations of electric and magnetic fields (see, for example, Griffiths [5]). This means that light has several properties that describe its physical attributes, including wavelength, direction of propagation, and direction of electric and magnetic field oscillation. The analysis of the wavelengths (or, equivalently, frequencies) of light is accomplished through spectroscopy. The polarization of light is most often defined to be the direction of oscillation of the electric field. This direction can be random with time, which can be called unpolarized light, or the time average can take on a preferential direction, which can be termed polarized light. The measurement of the polarization of light is accomplished with polarimetry. As an example, the equation for the electric field of linearly polarized light of frequency ω, propagating in direction k and polarized in some $\hat{n}$ is given below in Equation 1:

$$\vec{E} = \mathbb{R}\{E_o e^{i(\vec{k}\cdot\vec{r}-\omega t)}\hat{n}\}. \tag{1}$$

Spectroscopy

In order to make spectroscopic measurements, the range and intensities of wavelengths contained in a ray of light need to be analyzed. This is done by separating wavelengths spatially using a dispersive optical element. The dispersive element used in this instrument is a transmissive diffraction grating with a grating constant of $100l/\text{mm}$, meaning that the groove spacing is $1 \times 10^{-2}\text{mm}^{-1}$. Diffraction gratings are described by the grating equation, seen below in Equation 2 (for a more complete discussion of the following, see Pedrotti [6])

$$a(\sin\theta_i + \sin\theta_m) = m\lambda. \tag{2}$$

Where a is the grating constant, m is the integer order of diffraction, and θ_i and θ_m are the angles of incidence and diffraction, respectively. When the angle of incidence is zero the equation reduces to Equation 3

$$\sin\theta_m = \frac{m\lambda}{a}. \tag{3}$$

This causes an angular dispersion given by:

$$D = \frac{m}{a\cos\theta_m} = \mathrm{d}\theta_m/\mathrm{d}\lambda. \tag{4}$$

So at the sensor of a spectrograph the linear dispersion is given by Equation 5,

$$\frac{\mathrm{d}y}{\mathrm{d}\lambda} = fD \tag{5}$$

where f is the grating to sensor distance and D is the angular dispersion, and what is often called the plate scale is the inverse of the linear dispersion. In this instrument, the distance f was measured to be approximately 45.5mm. This, with a grating constant of $a^{-1} = 100l/\mathrm{mm}$ or $a = 1 \times 10^{-5}\mathrm{m} = 10^4\mathrm{nm}$, and using green light at 500nm leads to a 1^{st} order diffraction angle of

$$\theta_m = \arcsin\left(\frac{500\mathrm{nm}}{10^4\mathrm{nm}}\right) = 0.05\mathrm{rad}. \tag{6}$$

Therefore the angular dispersion is

$$\frac{1}{10^4\mathrm{nm} \times \cos(0.05)} = 1.00125 \times 10^{-4}\frac{\mathrm{rad}}{\mathrm{nm}}. \tag{7}$$

The linear dispersion, and thus plate scale then becomes

$$(1.00125 \times 10^{-4}\frac{\mathrm{rad}}{\mathrm{nm}} \times 45.5\mathrm{mm})^{-1} = 219.505\frac{\mathrm{nm}}{\mathrm{mm}}. \tag{8}$$

The camera used has a pixel pitch of $2.9\frac{\mu\mathrm{m}}{\mathrm{px}}$, so therefore the plate scale at the sensor becomes

$$fD = 219.506\frac{\mathrm{nm}}{\mathrm{mm}} \times 2.9 \times 10^{-3}\frac{\mathrm{mm}}{\mathrm{px}} = 0.6366\frac{\mathrm{nm}}{\mathrm{px}}. \tag{9}$$

Polarization of Light, Polarimetry, and Stokes Vectors

As mentioned before, the polarization of light is usually taken to be the direction of electric field oscillation (which also defines the direction of magnetic field oscillation, but most optics interact via electric field, and therefore it is most convenient to define it as such). Most familiar are linear and circular polarizations of light. In the first case, the time average of the electric field is found to be oscillating in a plane, in the second, the electric field traces out a helix such that, if observed along the direction of propagation, the electric field direction travels in a circle with time. The more

general case can be described as a combination of linear and circularly polarized states known as elliptically polarized light.

Note on Convention Used

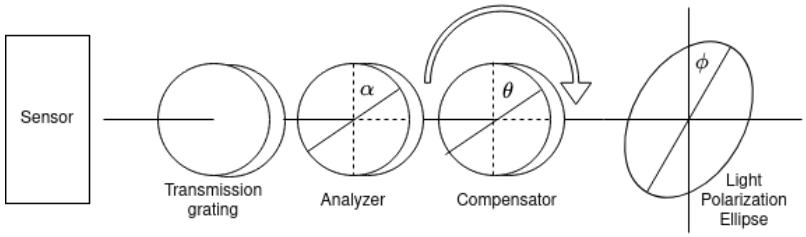

Figure 1: Optics and Angles Used in Convention

The important angles in the following discussion are the analyzer azimuth, the compensator fast axis azimuth, and the incident light polarization azimuth. The analyzer azimuth angle is the angle at which the polarizer transmits linearly polarized light. The compensator is a waveplate, which is constructed of a birefringent material. Birefringent materials essentially have two indexes of refraction, which defines an axes for the waveplate. Polarization components lying in one axis experience one index of refraction, and polarization components lying the other experience the second index of refraction. Thus, linear polarization that has components in both axis will experience transmittance through the waveplate at different speeds; one component is "retarded" relative to the other (hence why compensators are also called retarders), with the other progressing ahead in what is called the "fast axis". This is how waveplates can turn linear polarizations into circular or elliptical polarizations. Finally, the incident light azimuth is, for linear polarizations, the angle in a coordinate axis in which the linear polarization lies, or for elliptical polarization, the angle of the major axis of the ellipse.

There seemed to be no consistent convention used between sources as to how the compensator, analyzer, and incident light azimuth angles are defined. Similarly, there are multiple conventions used for Stoke's Vectors, and the Fourier coefficients described below are labeled differently according to sources. For example, Hauge & Dill [1] define the incident polarization azimuth to be α, the

compensator angle to be C, and the analyzer angle to be A, and use the convention of A_0, A_2, B_2, A_4, and B_4 for the Fourier coefficients. Berry, Gabrielse, & Livingston [7] use α and β for analyzer and compensator azimuths, respectively, and call the Fourier coefficients C_0, C_2, C_4, S_2, and S_4. The following conventions for Stokes parameters are also seen:

$$\mathbf{S} = \begin{bmatrix} I \\ Q \\ U \\ V \end{bmatrix} = \begin{bmatrix} I \\ M \\ C \\ S \end{bmatrix} = \begin{bmatrix} S_0 \\ S_1 \\ S_2 \\ S_3 \end{bmatrix} \tag{10}$$

where the first is seen in Keller [8], the second is seen in Berry, Gabrielse, & Livingston [7], and the third is seen in the chapter of Handbook of Optics by Chipman [9].

Care should be taken as to which convention is used, and in the following work the following convention has been established:

α: analyzer azimuth angle

θ: compensator azimuth angle

ϕ: incident azimuth angle

A_0, A_2, B_2, A_4, B_4: Fourier coefficients

S_0, S_1, S_2, S_3: Stokes Parameters

With this convention established, the quantities described above will be used in the following discussion of theory.

A common way to describe the intensities of polarized light is with a Stokes vector. A Stokes vector can be defined such that, given some defined coordinate system x and y [10]

$$\mathbf{S} = \begin{bmatrix} S_0 \\ S_1 \\ S_2 \\ S_3 \end{bmatrix} = \begin{bmatrix} E_x E_x^* + E_y E_y^* \\ E_x E_x^* - E_y E_y^* \\ E_x E_y^* + E_y E_x^* \\ i(E_x E_y^* - E_y E_x^*) \end{bmatrix}. \tag{11}$$

Described another way: The first parameter S_0 is the total intensity of the light, S_1 is the intensity of linearly polarized light in the vertical plane of the coordinate system, S_2 is the intensity of linearly polarized light in the plane 45^o rotated from the coordinate axis, and S_3 is the intensity

of circularly polarized light. For example:

$$\text{UP}: \begin{bmatrix} 1 \\ 0 \\ 0 \\ 0 \end{bmatrix} \text{LP,V}: \begin{bmatrix} 1 \\ 1 \\ 0 \\ 0 \end{bmatrix} \text{LP,H}: \begin{bmatrix} 1 \\ -1 \\ 0 \\ 0 \end{bmatrix} \text{LP,}+45^o\text{:} \begin{bmatrix} 1 \\ 0 \\ 1 \\ 0 \end{bmatrix} \text{LP,}-45^o\text{:} \begin{bmatrix} 1 \\ 0 \\ -1 \\ 0 \end{bmatrix} \text{RCP}: \begin{bmatrix} 1 \\ 0 \\ 0 \\ 1 \end{bmatrix} \text{LCP}: \begin{bmatrix} 1 \\ 0 \\ 0 \\ -1 \end{bmatrix} \tag{12}$$

where UP is (completely) Unpolarized Light; LP,V is Linearly Polarized Vertical light; LP,H is Linearly Polarized Horizontal light; LP,$+45^o$ is Linearly Polarized light at +45 degrees; LP, -45^o is Linearly Polarized light at -45 degrees; RCP is Right Circularly Polarized light; and LCP is Light Circularly Polarized light.

Polarized light is also described in terms of ellipticity χ, in which the azimuth orientation ϕ is along the major axis of the ellipse ($\chi = 0$ for linear polarizations, $+/-\pi/4$ for circularly polarized light, etc). Polarized light can also be only partially polarized, and thus a Degree of Polarization (DOP) quantity is also defined (it also sometimes useful to talk about the Linear Degree of Polarization and Circular Degree of Polarization. All Stokes vectors above are perfectly polarized light except the first one, which is perfectly unpolarized. In terms of Stokes parameters [9],

$$\begin{aligned} \chi &= \frac{S_3}{S_0 + \sqrt{S_1^2 + S_2^2}} \\ \phi &= \frac{1}{2} \arctan \frac{S_2}{S_1} \\ \text{DOP} &= \frac{\sqrt{S_1^2 + S_2^2 + S_3^2}}{S_0} \\ \text{DOP}_{\text{lin}} &= \frac{\sqrt{S_1^2 + S_2^2}}{S_0} \\ \text{DOP}_{\text{circ}} &= \frac{S_3}{S_0}. \end{aligned} \tag{13}$$

Mueller matrices are a matrix description of polarization-modifying optics. A Mueller matrix operates on a Stokes vector to produce another, transformed vector. For example, the Mueller matrix for a linear polarizer is given by [9]

$$\mathbf{L} = \begin{bmatrix} 1 & \cos(2\alpha) & \sin(2\alpha) & 0 \\ \cos(2\alpha) & \cos^2(2\alpha) & \cos(2\alpha)\sin(2\alpha) & 0 \\ \sin(2\alpha) & \cos(2\alpha)\sin(2\alpha) & \sin^2(2\alpha) & 0 \\ 0 & 0 & 0 & 0 \end{bmatrix} \tag{14}$$

where α is the orientation of the linear polarizer in some coordinate axis. The Mueller matrix for a linear retarder of retardance δ with fast axis oriented along θ is given by [9]

$$\mathbf{R} = \begin{bmatrix} 1 & 0 & 0 & 0 \\ 0 & \cos^2(2\theta) + \sin^2(2\theta)\cos(\delta) & \cos(2\theta)\sin(2\theta)(1-\cos(\delta)) & \sin(2\theta)\sin(\delta) \\ 0 & \cos(2\theta)\sin(2\theta)(1-\cos(\delta)) & \cos^2(2\theta)\cos(\delta) + \sin^2(2\theta) & -\cos(2\theta)\sin(\delta) \\ 0 & -\sin(2\theta)\sin(\delta) & \cos(2\theta)\sin(\delta) & \cos(\delta) \end{bmatrix} \tag{15}$$

where $\delta = \pi/2$ for a quarter waveplate.

For this instrument, there is a rotating quarter waveplate followed by a fixed linear polarizer. In terms of matrix algebra, the polarimetric response of the instrument can described by setting $\alpha = \text{const} \equiv 0$, $\delta = \pi/2$ and defines the coordinate axis, and allowing θ to vary from 0 to 2π. Some example response curves can be seen in the following graphs, which were computed and plotted in MATLAB.

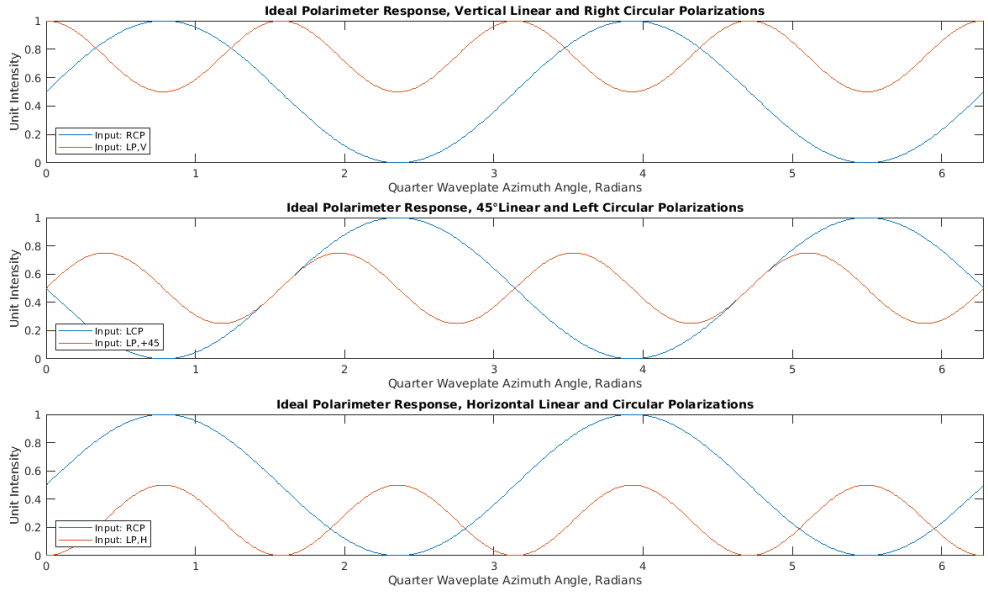

Figure 2: Polarimeter Response. The first graph plots $\mathbf{L} \cdot \mathbf{R} \cdot \mathbf{S}_{LP,V}$ and $\mathbf{L} \cdot \mathbf{R} \cdot \mathbf{S}_{RCP}$. The second graph plots $\mathbf{L} \cdot \mathbf{R} \cdot \mathbf{S}_{LP,+45}$ and $\mathbf{L} \cdot \mathbf{R} \cdot \mathbf{S}_{LCP}$. The third graph plots $\mathbf{L} \cdot \mathbf{R} \cdot \mathbf{S}_{LP,H}$ and $\mathbf{L} \cdot \mathbf{R} \cdot \mathbf{S}_{RCP}$. These graphs are similar to those generated by Hauge & Dill [1].

Note that the circular polarization input takes the form of a sinusoid with a frequency twice that to the compensator rotational frequency, and the linear polarization input takes the form of a sinusoid with a frequency four times that of the compensator frequency. This fact is reflected in

the following mathematics, starting with the general equation for such a polarimeter, seen below in Equation 17, in terms of the Stokes parameters S_0, S_1, S_2, S_3, (Berry, Gabrielse, & Livingston, [7]),

$$\begin{aligned} I(\theta) = \frac{1}{2}\left[S_0 + \left(\frac{S_1}{2}\cos 2\alpha + \frac{S_1}{2}\sin 2\alpha\right)(1+\cos\delta)\right] + \frac{1}{2}S_3 \sin\delta \sin(2\alpha - 2\theta) \\ + \frac{1}{4}\left[(S_1\cos 2\alpha - S_2 \sin 2\alpha)\cos 4\theta + (S_1 \sin 2\alpha + S_2 \cos 2\alpha)\sin 4\theta\right](1-\cos\delta) \end{aligned} \tag{16}$$

where α is the analyzer azimuth, θ is the azimuth of the waveplate fast axis, and δ is the retardance of the waveplate. If we take the analyzer azimuth to define the coordinate axis, i.e., defining $\alpha \equiv 0$, the equation reduces (with some rearranging of terms) to the following, as seen in Keller [8]

$$I(\theta) = \frac{1}{2}[S_0 + \frac{S_1}{2}[(1+\cos\delta) + (1-\cos\delta)\cos 4\theta] + \frac{S_2}{2}(1-\cos\delta)\sin 4\theta - S_3 \sin\delta \sin 2\theta]. \tag{17}$$

This equation can be simplified by assuming the use of an ideal quarter waveplate, $\delta = \pi/2$rad, resulting in the following equation

$$I(\theta) = \frac{1}{2}\left[S_0 + \frac{1}{2}(1 + S_1\cos 4\theta + S_2 \sin 4\theta) + S_3 \sin 2\theta\right]. \tag{18}$$

Again, where θ is the compensator azimuth angle. Compare this equation to the graphs generated in Figure 2. Berry, Gabrielse, & Livingston notes that Equation 16 takes the form of a Fourier series [7], as seen in Equation 19,

$$I(\theta) = A_0 + A_2\cos 2\theta + B_2 \sin 2\theta + A_4 \cos 4\theta + B_4 \sin 4\theta \tag{19}$$

which is also reported by Hauge & Dill [1], defining the following coefficients in terms of arbitrary α, ϕ, and χ, but assuming an ideal quarter waveplate $\delta = \frac{\pi}{2}$rad:

$$\begin{aligned} A_0 &= 2 + \cos 2\chi \cos 2(\alpha - \phi) \\ A_2 &= 2\sin 2\chi \sin 2\alpha \\ B_2 &= -2\sin 2\chi \cos 2\alpha \\ A_4 &= \cos 2\chi \cos 2(\alpha + \phi) \\ B_4 &= \cos 2\chi \sin 2(\alpha + \phi). \end{aligned} \tag{20}$$

Followed the established convention, θ is the azimuth angle of the compensator fast axis, α, is the azimuth angle of the analyzer, and ϕ and χ is the azimuth and ellipticity of the incoming light. For

example, as done in previous equations α could define the coordinate axis and therefore be defined to be 0. Therefore for vertical linearly polarized light (i.e., $\phi = 0$, $\chi = 0$) this reduces to (within a multiplicative constant)

$$I_{\text{lin}}(\theta) = 3 + \cos(4\theta). \tag{21}$$

Similarly, for circularly polarized light, where $\chi = \pi/4\text{rad}$

$$I_{\text{circ}} = 2 - 2\sin 2\theta. \tag{22}$$

The fact that the instrument response takes the form of a Fourier series described by Equation 19 lends itself to the idea of a Fourier analysis of the signal, and is the operating principle behind the Fourier polarimeter: the modulated signal is sampled at compensator azimuth angles θ, and can then be analyzed to obtain the Fourier coefficients that describe the light. These Fourier coefficients can be used to determine the Stokes parameters [7], as seen by the below Equations 23. This is the principle of operation behind the commercially available Thorlabs PAX1000 polarimeter [11]

$$\begin{aligned}
S_0 &= A_0 - \frac{1+\cos\delta}{1-\cos\delta}[A_4\cos(2\alpha+4\theta_0) + B_4\sin(2\alpha+4\theta_0)] \\
S_1 &= \frac{2}{1-\cos\delta}[A_4\cos(2\alpha+4\theta_0) + B_4\sin(2\alpha+4\theta_0)] \\
S_2 &= \frac{2}{1-\cos\delta}[B_4\cos(2\alpha+4\theta_0) - A_4\sin(2\alpha+4\theta_0)] \\
S_3 &= \frac{A_2}{\sin\delta\sin(2\alpha+4\theta_0)} = \frac{-B_2}{\sin\delta\cos(2\alpha+4\theta_0}.
\end{aligned} \tag{23}$$

Constraints and Design Choices

There are two aspects to a spectropolarimeter: the part that allows for spectroscopic analysis of light, and the part that allows for a measurement of the polarization state. There are many ways to go about both of these tasks, each with their advantages and disadvantages. For example, to make a spectroscopic measurement, a dispersive element is required. This can take the form of a prism or arrangement of prisms, or a diffraction grating, which can take the form of either a reflective grating or a transmissive grating. With a reflection grating, grooves are highly reflective, and the dispersion comes from light reflected off of the grooves; in a transmission grating, however, a clear glass blank has grooves etched into the surface, acting as an opaque mask, and the transmitted light is dispersed. See, for example, Pedrotti, Chapter 12 [6] for more information on diffraction gratings. A prism has the advantage of higher spectrum throughput; however, they also have an inherently nonlinear wavelength response. Gratings inherently are more nearly linear, but lose much spectral sensitivity to the 0^{th} order image. This can be mitigated somewhat with blazed gratings. Spectrographs also can be of slitless designs or designs able to accommodate entrance slits.

For polarimetric measurement, some arrangement of a linear polarizer (in this context, often referred to as an analyzer) and phase modifying optic is often used (for example, a quarter-waveplate, often called a retarder or compensator). These types of polarimeters require that one of the optical elements (analyzer or compensator) rotates, and the result is a modulated signal that can be analyzed in terms of frequency components and are thus sometimes called Fourier polarimeters. These polarimeters have the advantage of being able to provide precise, full polarization state measurements, as well as being insensitive to other optical abberations and imaging field flatness. The disadvantages of such polarimeters, aside from the inherent mechanical complexity associated with the requirement for a rotating optic, include the inability to provide instantaneous polarization measurements for rapidly changing polarization states (measurements are made within some time Δt dependent on the rotational frequency of the optic and the sampling rate of the sensor), as well as possible influence of atmospheric turbulence for slowly modulated signals [Inst. for Ast. Specpol, Keller].

In order to acquire enough signal to overcome noise thresholds in astronomical data, long exposures are often required. With this consideration, the choice to use a Fourier polarimeter design was made, with the understanding that only constant or slowly changing polarization states would

be measurable. The design of the polarimeter part of this spectropolarimeter follows a rotating compensator, fixed analyzer design, which mitigates any polarization dependence in the sensor.

Transmission gratings are available from various optic suppliers such as Thorlabs and Edmund Optics, in both transmission and reflection forms, of various ruling densities. The decision was made to use a transmission grating, as the reflection gratings are often unmounted and the additional mounting hardware was not conducive to the construction of this instrument. Additionally, reflection gratings change the direction of the optical path significantly, complicating the design. A transmission grating allows for a less complex straight-through optical path, so long as the dispersion angle is not too great.

Therefore, the optical train for this spectropolarimeter, following the telescope back and/or focal reducer, is a rotating quarter waveplate, a fixed linear polarizer, and a fixed transmission diffraction grating of $100l$/mm, followed by the camera sensor.

Selection of Optics

In selecting optics for such a project there are many things to consider, including size, optical material, performance across the desired wavelengths, and especially price.

For this project, an effort to use as many off-the-shelf parts was made between the commonly available astronomical components standards and the common optical components standards. Additionally, cost of components was a considerable factor in selected parts and design. Amateur astronomical components often use 2 inch or 1.25 inch slip fit connections with internal threads for filters or T-mount connections, while optical lab components often come in 2 inch or 1 inch varieties to accommodate 2 or 1 inch optical tubes with provision for use on optical breadboards or in cage mount systems. Funding for this project was generously made possible by the University of Maine Center for Undergraduate Research (CUGR) in the amount of $1,100.00 and the Physics Department Kreuger Fund in the amount of $562.00 bringing the total budget for this project to $1662.00.

The telescope used for the duration of this project was a standard Celstron C9.25, a 9.25 inch (235mm) aperture, 2350mm focal length, F/10 Schmidt Cassegrain Telescope (SCT). A focal reducer was used for much of the work, which brought the focal length down to 1480.5mm and F/6.3. This optical tube was used because it was in the author's possession and is representative of typical (although modest) instrumentation that would be available to amateurs or institutions with limited budgets.

The necessary optics for this instrument, aside from the optical tube collecting light, are a linear polarizer, a $\lambda/4$ waveplate, and a transmission grating. Each of these components can vary in price and quality, and therefore tradeoff considerations must be made in selecting components.

The linear polarizer used was a 25mm glass substrate dichroic polarizer from Edmund Optics. Of the commonly available options of plastic dichroic, glass dichroic, and wire grid polarizers, the glass polarizer was chosen for superior image quality, high extinction ratio, and reasonable price. The plastic polarizer was of comparable polarization performance and cheaper, but was avoided in an effort to preserve image quality as much as possible. The wire grid polarizers, in addition to being more expensive, were advertised with a higher wavelength dependence to polarization extinction ratio. See Figures 3, 4, and 5 below.

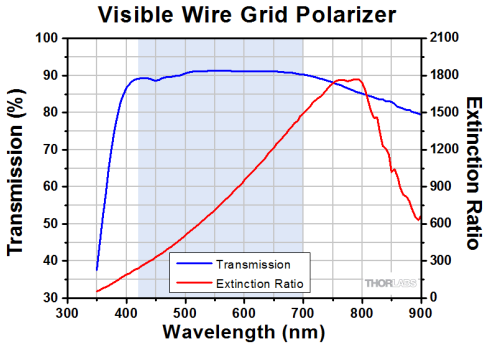

Figure 3: Wire Grid Polarizer
(Source: ThorLabs)

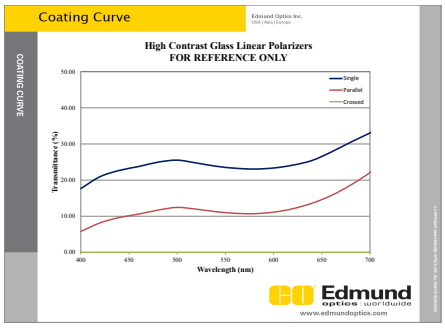

Figure 4: Glass Dichroic
(Source: Edmund Optics)

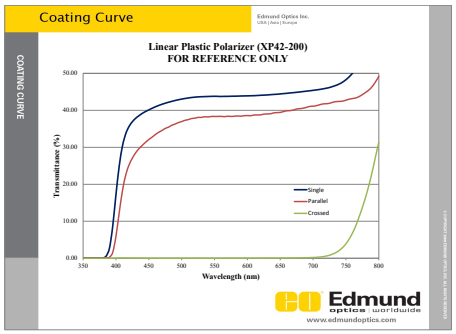

Figure 5: Plastic Dichroic
(Source: Edmund Optics)

Similar considerations must be made for quarter waveplates. These optics are often expensive and most are made for nonachromatic purposes. Achromatic waveplates are quite expensive, for

example, see the quartz achromatic quarter /4 waveplate from Edmund Optics 46-558 at $825.00. However, costs can be kept lower by using a polymer waveplate, such as the achromatic polymer waveplate used in this project, Edmund Optics 88-198, which claims achromatic performance from 450-600nm.

Mounted transmission gratings with threaded housings for astronomical cameras already exist in 100l/mm and 200l/mm in the form of the Star Analyser SA-100 and SA-200 models. In this case, the 100l/mm model was already in possession and was used.

Optomechanics

Use of standard 30mm and 60mm optical cage products were used to construct much of the instrument. Although all optics purchased were 1 inch in diameter, the larger 60mm cage structure was utilized to construct the framework to support the electromechanics used in the polarimetry.

The interface between the Schmidt Cassegrain threads and the spectropolarimeter is done with a SCT thread to T-mount adapter, and then a Thorlabs T-Mount to SM1 adapter which converts the interface to standard optical lab components. This interfaces to the 30mm to 60mm cage plate, where 1 inch posts at the 30mm system attaches the rotating mount to the cage plate and the 60mm system holds the custom cut brackets for the motor, bearing, and potentiometer. The system is then converted back to 1.25 inch astronomical slip fit connection for connecting the camera. The camera has capability to interface directly to a T-Mount thread via adapter, which would be more mechanically sound; however, the diffraction grating used was a pre-mounted transmission grating with threads for standard 1.25" astronomical nosepiece, and therefore the conversion to the 1.25" standard was made.

A 1" long, 1" diameter optic tube was screwed in to the rotation mount as well, to provide a surface with which to interface to the electromechanics, discussed in the next section.

Electromechanics

To make a polarimetric measurement, the $\lambda/4$ waveplate must rotate relative to the other optics. The rotation optic mount from Thorlabs provides a smooth, well damped rotation housing for an optic; however, it has no provision for motorized control. To allow for motorized rotation, two problems must be addressed: 1. the optical path cannot be obstructed. 2. The motor must turn the optic to specific, measurable angles. Problem 1 means that the motor and associated mechanics must be adjacent to the axis of rotation, not inline with it. Problem 2 would suggest that a servo of

some kind should be applied. Commonly available servos are often limited to less than 360 degrees, meaning that in order to get a full rotation at the optic (in a 1" optical tube) the shaft on the servo must have a pulley or gear with a diameter of 1" or greater. Instead of purchasing a servo that meets the torque, range of motion, and price constraints, the decision was made to implement a multi-turn servo to turn the optic. This has several advantages: first, a multi turn servo would allow for the pulley or gear to have a smaller diameter, making the arrangement less bulky and easier to work around. Second, for a servo that makes multiple turns for a single turn at the optic, the uncertainty and precision in the angle of the servo shaft is reduced proportionally at the optic. Therefore, a higher precision can be attained by measuring the servo shaft angle instead of the optic azimuth angle. Finally, an angle measurement is required to address Problem 2 discussed earlier, and the feedback necessary to control the motor would provide this.

The construction of this optomechanical servo required a geared DC motor, an H-Bridge motor controller, a 10 turn potentiometer, and an analog to digital converter to read the signal with a Raspberry Pi computer. The only constraint on the motor was that it have enough torque and had characteristics that made it controllable. The Geartisan 12V motor comes in several gear models with different torque and RPM specifications; the 5RPM, 10 Kg-cm model was chosen for its adequate torque and slow shaft rotation. In a tradeoff between speed and precision, precision is preferred, so although the 100RPM, 4.5 Kg-cm model was found to have enough torque, the slower one was used in an effort to increase precision. An early prototype attempted to use an ungeared, 13360RPM 0.154 Kg-cm motor which was found to not have enough torque.

A toothed belt and pulley system was chosen to ensure no slip between the motor and the optic, with parts ordered from SDP/SI. The 72 tooth plastic pulley was hollowed out and fitted to an aluminum adapter fitted with setscrews, see Figure 6. This adapter was the diameter of the 1" optical tube, and thus could be securely tightened to the optical tube, see Figure 7

Figure 6: 72 Tooth Pulley, Modified

Figure 7: 72 Tooth Pulley, Modified, on Rotation Housing (also shown: SCT to T-Mount, T-Mount to SM1, and 30mm/60mm Cage Plate)

On the motor shaft, a smaller 18 tooth pulley with 6mm bore was affixed to an aluminum, 6mm axle with epoxy. The other side of the 6mm bore was left to attach to the 6mm motor shaft via setscrew. See Figure 8

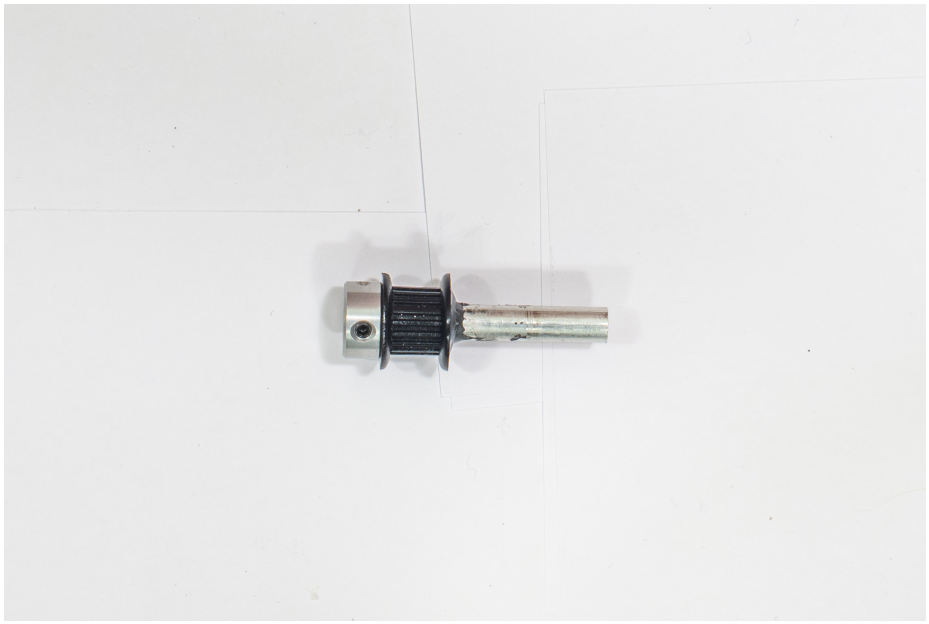

Figure 8: 18mm Tooth Pulley, Modified with Aluminum Axle

The axle passes from motor shaft, to the 18 tooth pulley, into a ball bearing to support the tension of the belt, and finally on to a 10 turn 5kΩ potentiometer. The motor, bearing, and potentiometer are supported and attached to the 60mm optical cage system by 1/4" aluminum brackets, which were custom designed and water-jet cut. See Figure 9.

Figure 9: Water-Jet Cut Brackets Interfacing to 60mm Optical Cage System for: 10 Turn Potentiometer, Ball Bearing, Motor

To make a measurement set, it is necessary to turn the optic to a measured angle, take a camera exposure, and move to the next angle, and repeat. The goal was to have this be a completely automated system, where the camera and motor would act synchronously via program using the camera SDK. However, due to time constraints and trouble working with the SDK, the automated aspect of the instrument was not implemented, and camera and motor triggering were done manually via separate programs.

Motor Control and Calibration

The motor control system can be represented by the following figure, Figure 10:

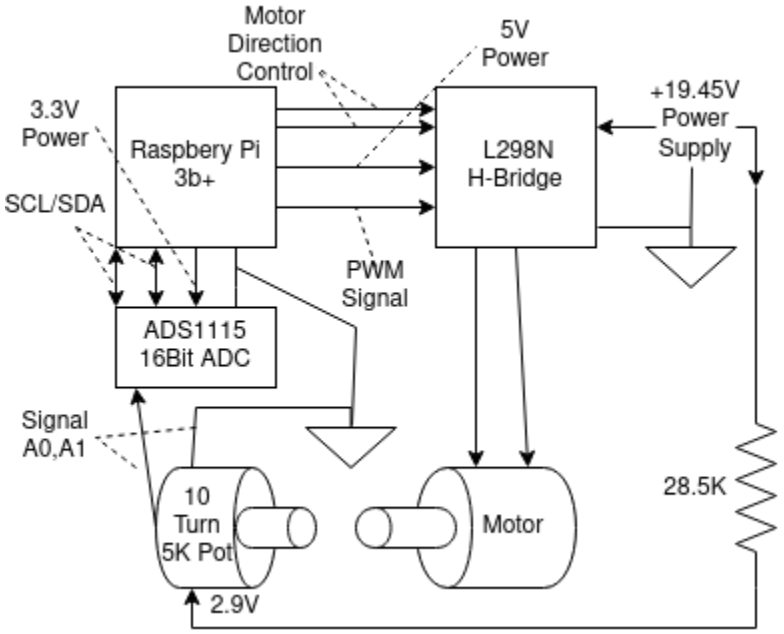

Figure 10: Motor Control Schema

The General Purpose Input/Output (GPIO) pins of the Raspberry Pi cannot supply enough current to drive an inductive load, such as the motor. Therefore, an H-bridge is used to take a digital signal from the GPIO pins and apply power accordingly to the motor from an external power source, in this case a 19.45V power supply. The input to the H-bridge can be a Pulse Width Modulated (PWM) signal, allowing for variable speed control. To determine the position of the motor, the shaft is attached to the 10-turn potentiometer. A reference voltage of 2.9V was used across the 5K potentiometer; this voltage was supplied from the motor power supply and reduced with series resistors in a voltage divider. It should be noted that the digital reference voltage of the Raspberry Pi was tried as a reference voltage, but was found to be too noisy. The ADS1115 Analog

to Digital Converter (ADC) reads the voltage across the potentiometer, and sends a digital signal to the Raspberry Pi.

The control structure for the motor is an error-proportional control. In this control structure, some error ϵ is read as a difference in desired position and measured position:

$$\epsilon = P_{\text{desired}} - P_{\text{measured}} \tag{24}$$

Once the error is determined, a voltage proportional to the voltage is sent to the motor. In this case, this means that a PWM signal with a duty cycle proportional to error by some constant $\epsilon \cdot K_p$ is sent to the H-Bridge, effectively applying a proportional voltage to the motor. It was found that the motor stalled at a PWM duty cycle lower than 18 (range of 0-100). A K_p of 0.3 was found to be effective, within the range of error between 250 and 60 digital values. Above this range, a constant duty cycle of 75 is applied, and below this range a constant duty cycle of 18 is applied. The Raspberry Pi reads the ADS1115 samples continuously and adjusts PWM duty cycle accordingly until 0 error is reached. It was found that this worked with minimal overshoot or ringing, and therefore it was decided that more complex terms (for example, integral proportional or derivative proportional terms) were unnecessary. The actual position after the motor stopped moving was found to be usually within 20 digital values; however, in this application it is not the precisely specific position that is important, only that it can be measured accurately and precisely.

The relation between the reported digital value from the ADC and the angle of the optic was determined in the following manner. With the motor shaft disconnected from the system, but the optic and potentiometer connected, 5 measurements of the angle 0 were made by eye using the engraved scale on the optic rotation housing, deviating and returning after each measurement and recording the ADC value. The same procedure was done for $+20^o, -20^o, +90^o, -90^o, +180^o$ and -180^o. For each of these measurements, the result was averaged, and the difference from the 0 position measurement was found. This difference was divided by the corresponding deviation in degrees, thus finding the conversion factor of digital value per degree at optic. This process was repeated for angles 360^o away, providing a set of measurements in a different range on the potentiometer. These numbers are reported in the Tables 1 and 2 below, along with the standard deviation of the measurements.

Degrees:	0	+20	-20	+90	-90	+180	-180
Digital Reading:	16421	15898	16941	14590	18786	11714	21129
·	16420.5	15900	16940	14594	18781.5	11719	21129
·	16425	15901	16935	14594	18786	11709	21135
·	16422	15901	16936	14589	18787	11709	21130
·	16421	15896	16936	14590	18781	11719	21130
Average Reading:	16421.9	15899.2	16937.6	14591.4	18784.3	11714.0	21130.6
Standard Deviation:	$\sigma : 1.82$	$\sigma : 2.17$	$\sigma : 2.70$	$\sigma : 2.41$	$\sigma : 2.82$	$\sigma : 5.00$	$\sigma : 2.51$
Conversion Factor:	0	26.12	25.78	20.34	26.25	26.16	26.16

Table 1: Calibration of Motor Angle. Includes: recorded digital values for each angle location, the average value of the set, the standard deviation of the set, and the conversion factor found from that angle (average reading/degrees)

Degrees:	0	+20	-20	+90	-90	+180	-180
Digital Reading:	7009	6485	7525	5182	9372.5	2312	11714
·	7008.5	6490	7529	5181	9373	2313	11708
·	7014	6490	7529	5181	9377	2318	11719
·	7020	6491	7529	5181.5	9382	2327	11719
·	7020	6501	7529	5171	9383	2318	11719.5
Average Reading:	7014.3	6491.4	7528.2	5179.3	9377.5	2317.6	11715.9
Standard Deviation:	$\sigma : 5.63$	$\sigma : 5.86$	$\sigma : 1.79$	$\sigma : 4.66$	$\sigma : 4.90$	$\sigma : 5.94$	$\sigma : 4.59$
Conversion Factor:	0	26.15	25.69	20.39	26.26	26.09	26.12

Table 2: Calibration of Motor Angle, Range 2. Includes: recorded digital values for each angle location, the average value of the set, the standard deviation of the set, and the conversion factor found from that angle (average reading/degrees)

Note that in each set, the measurement for $+90^o$ is a distinct outlier[1]. The conversion factors were averaged with and without the outlier for each set, and are reported below, along with the average standard deviation of the set, as seen in the table below. For use in controlling motor, it was decided to use the average without the outlier, and the average value 26.1 values/degree at optic was used. The average standard deviation was used (after conversion to degrees or radians) as a measure of uncertainty in the angle of the optic.

Average w/Outlier	Average w/o Outlier	Average σ
25.14	26.10	2.77
25.12	26.06	4.12
25.13	26.08	3.45

Table 3: Average Conversion Factors and Standard Deviation from Both Ranges

[1]At a later date, the author remeasured the angles 0 and +90, as well as +70. Both new measurements resulted in conversion factors of 26.1. Given that the measurement reported for +90 in these tables would actually line up very well with +70, it is most likely that the measurements made here were, in reality, of +70 not +90

Parts Used

1. Thorlabs CRM1/M Inline Cage Assembly Rotation Mount
2. Thorlabs TMA1 SM1 Ext to TMount Int Adapter (2x)
3. Thorlabs LCP02/M 30mm to 60mm Cage Plate (2x)
4. Thorlabs SM1l10 St 1" Lens tube, 1" length
5. Thorlabs ER1 (1") and ER6 (6") (4x each)
6. M42x0.75 Male Thread to 1.25" adapter
7. Edmund Optics Tech Spec Glass Linear Polarizer 25mm
8. Edmund Optics Polymer Retarder 1/4 450nm-600nm 25mm
9. Star Analyser SA-100 diffraction grating
10. ZWO ASI290mm Camera
11. SDP/SI MXL 18 tooth pulley
12. SDP/SI MXL 72 tooth pulley
13. SDP/SI MXL toothed belt
14. SDP/SI 6mm Flange Mounted Ball Bearing
15. Custom cut motor, bearing, and potentiometer brackets
16. Greartisan DC 12V 5RPM Geared Motor
17. McMaster-Carr 60845K31 Two-Piece Shaft Coupling
18. 10 turn 5K potentiometer
19. Celestron SCT to T-Mount Adapter
20. ADS1115 16 Bit ADC
21. L298N H-Bridge Motor Driver
22. Raspberry Pi (3b+)

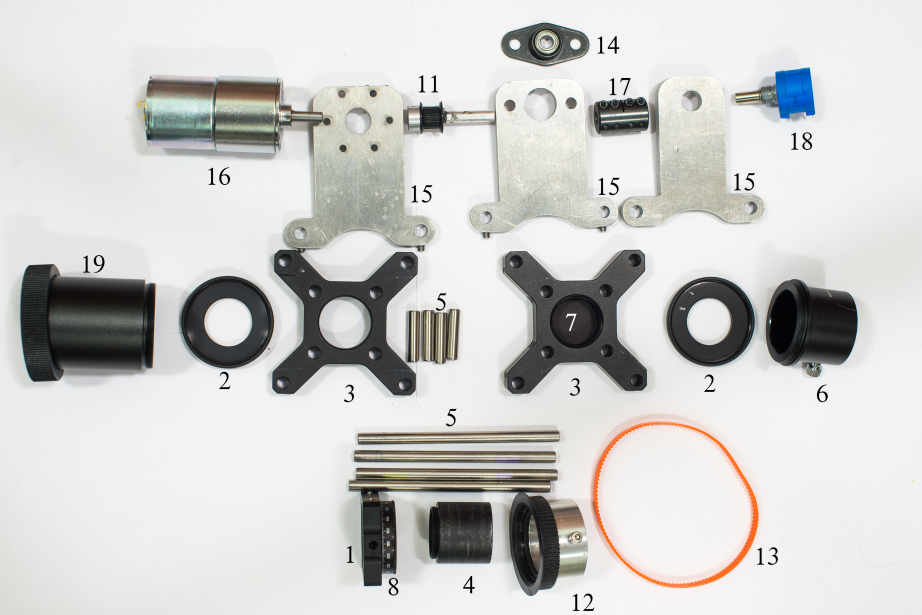

Figure 11: Parts used. Missing: Raspberry Pi, ADS1115 ADC, L298N H-Bridge, ZWO ASI290mm and SA100 diffraction grating

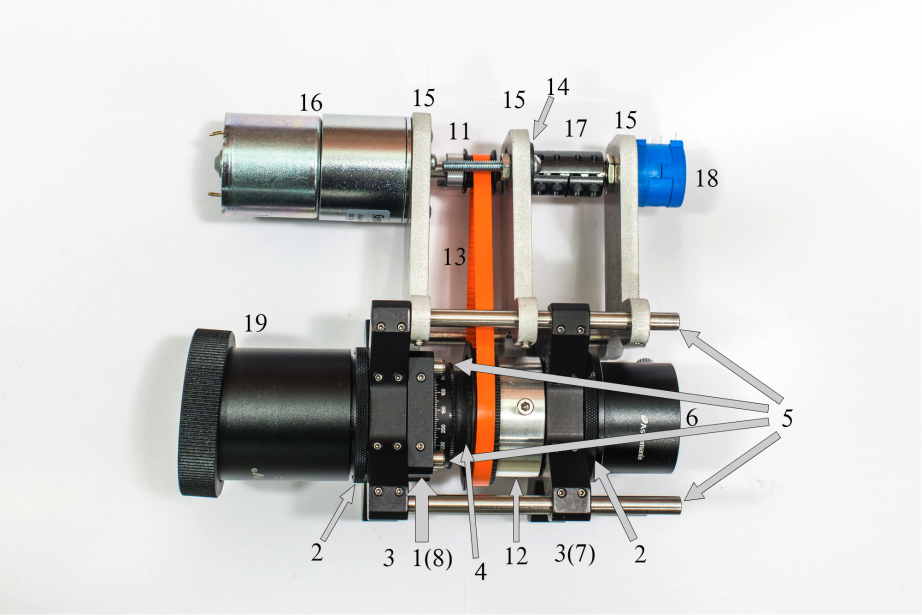

Figure 12: Assembled Spectropolarimeter, internal optics in parenthesis. Note: the leftmost interface is a loose collar, and is not an angled piece

Figure 13: Assembled Spectropolarimeter, In Use

RESULTS

Controlled Calibration

In order to test the polarimetric response of the instrument, linear and circularly polarized light were generated and measured. This was accomplished by setting an LED covered by a pinhole mask and behind a photographic polarizing filter at one end of a room, with the telescope (9.25" SCT) and spectropolarimeter set up on the other side. For these calibration tests, the 9.25" SCT operated at F/6.3. Measurements were made at 10^o intervals from $0^o - 360^o$. To process the data, the frames were read into MATLAB, where the Region of Interest (ROI), in this case the spectrum of the LED, was isolated. For example, the frames from the linear polarization measurement are seen below, in Figure 14. The average pixel intensity value was found for each frame, and plotted to the corresponding angle that was recorded from the motor for that frame. The intensity plot for the linear polarization measurement can be seen in Figure 15. A sine curve fit can be seen in 16.

For all following plots: horizontal error bar shows an average one standard deviation of the motor position reported in Table 3 converted to radians, but scaled 10 times to be visible (0.02 radians instead of 0.002 radians). The vertical error bars represent the RMSE reported from the MATLAB curve fitting goodness-of-fit.

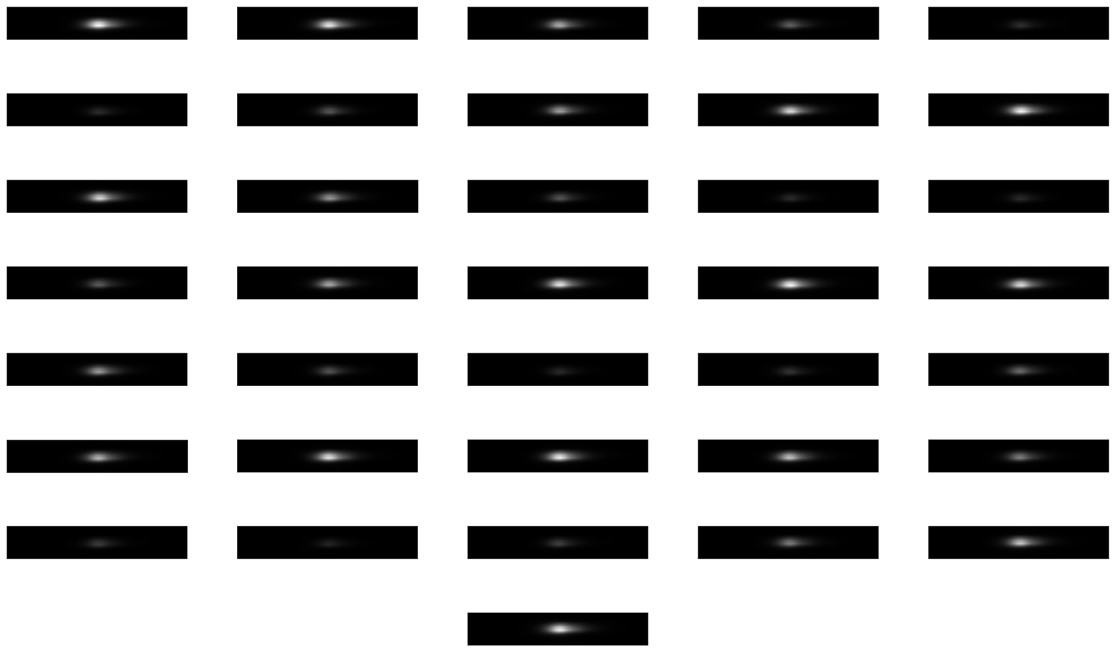

Figure 14: Linear Polarization Filter ROI Frames, 251x46 pixels. Starting top, left to right, 10^o increments: Angles 0^o-40^o, 50^o-90^o, 100^o-140^o, 150^o-190^o, 200^o-240^o, 250^o-290^o, 300^o-340^o, 350^o

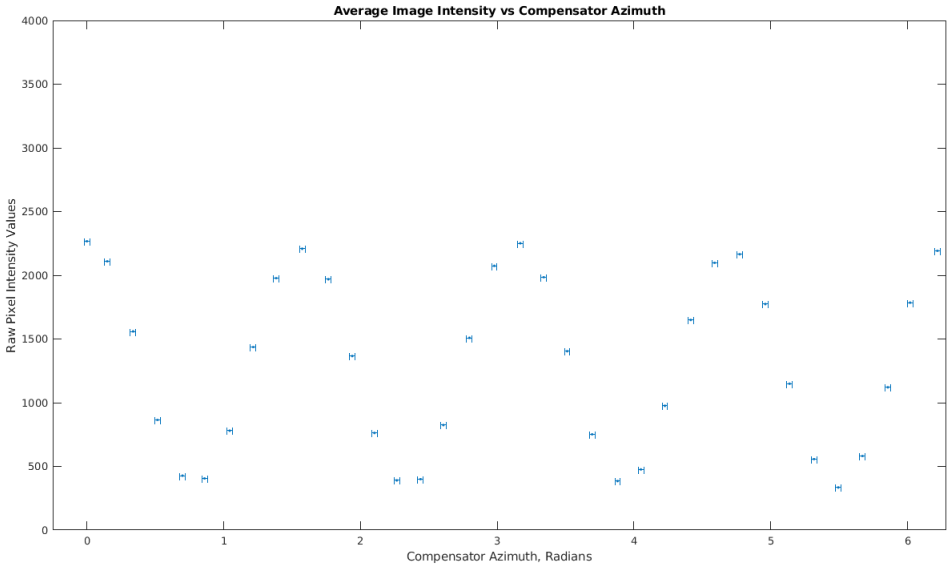

Figure 15: Intensity Plot, Linear Polarization Calibration, Horizontal Error Bars Scaled 10x

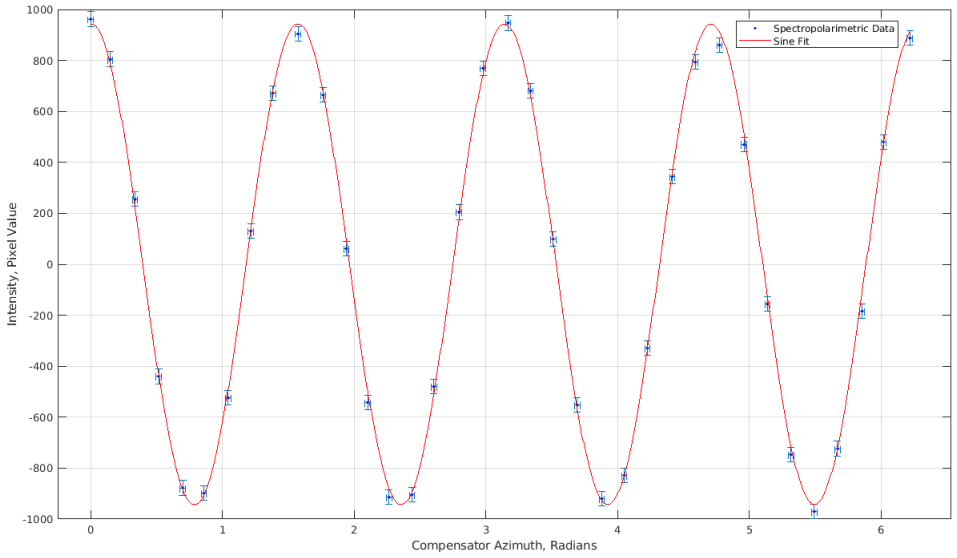

Figure 16: Sine Curve Fitted Data, Linear Polarization Calibration, Horizontal Error Bars Scaled 10x

Curve fit results: General model: a1*sin(b1*x+c1)

Coefficients (with 95% confidence bounds):

a1 = 942.8 (929.2, 956.4); b1 = 4.005 (3.997, 4.014); c1 = 1.557 (1.527, 1.586);

Adjusted R Squared = 0.9983; RMSE = 28.5843

The same procedure was followed for the circular polarization input. Figures 17,18, and 19 show intensity plots, a sine curve fit, and a two term sum of sine curve fit, respectively. The frames are not shown here but are similar in nature to those seen in the linear polarization frames in 14.

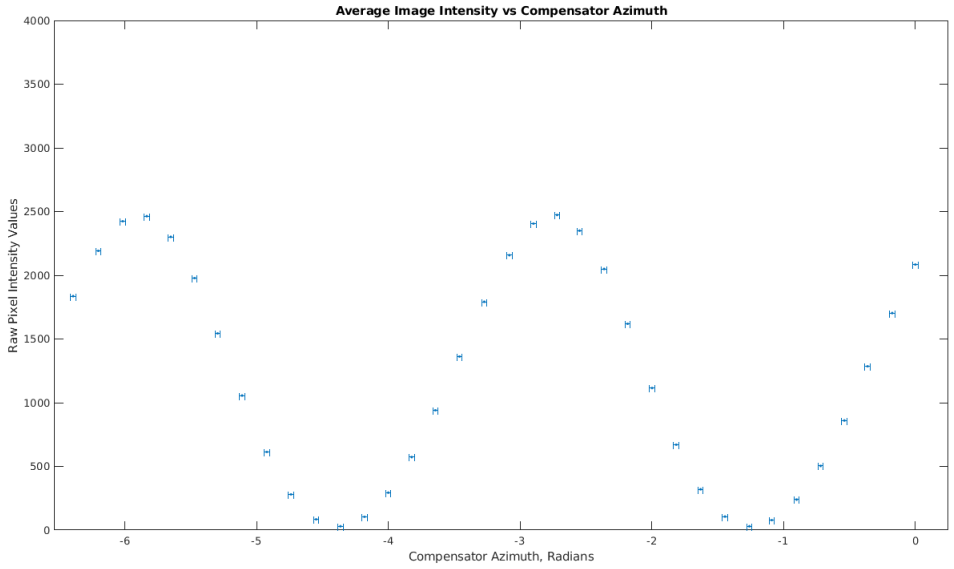

Figure 17: Intensity Plot, Circular Polarization Calibration, Horizontal Error Bars Scaled 10x

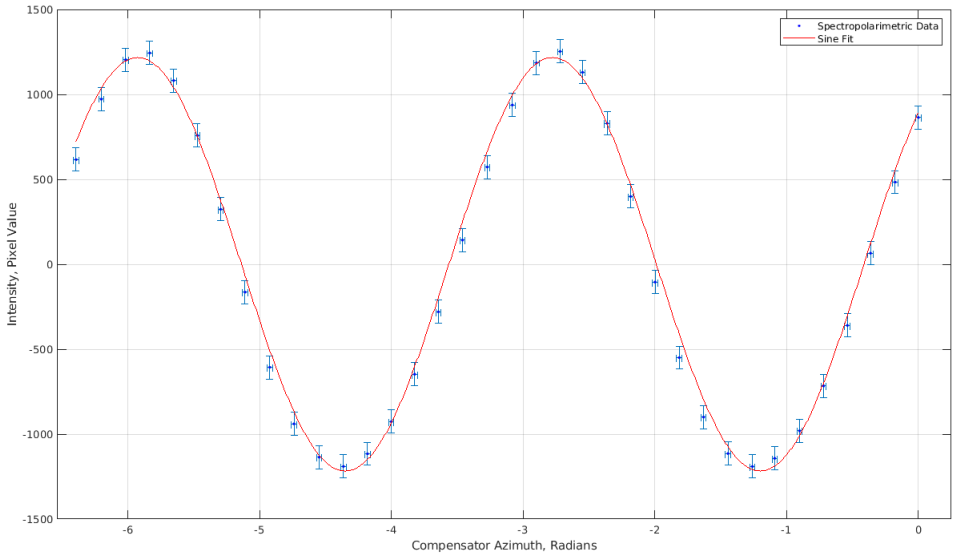

Figure 18: Sine Curve Fit, Circular Polarization Calibration, Horizontal Error Bars Scaled 10x

Curve fit results: General model: a1*sin(b1*x+c1)

Coefficients (with 95% confidence bounds):

a1 = 1217 (1184, 1250); b1 = 1.994 (1.98, 2.009); c1 = 0.8246 (0.7747, 0.8745);

Adjusted R Squared = 0.9939, RMSE = 68.2040

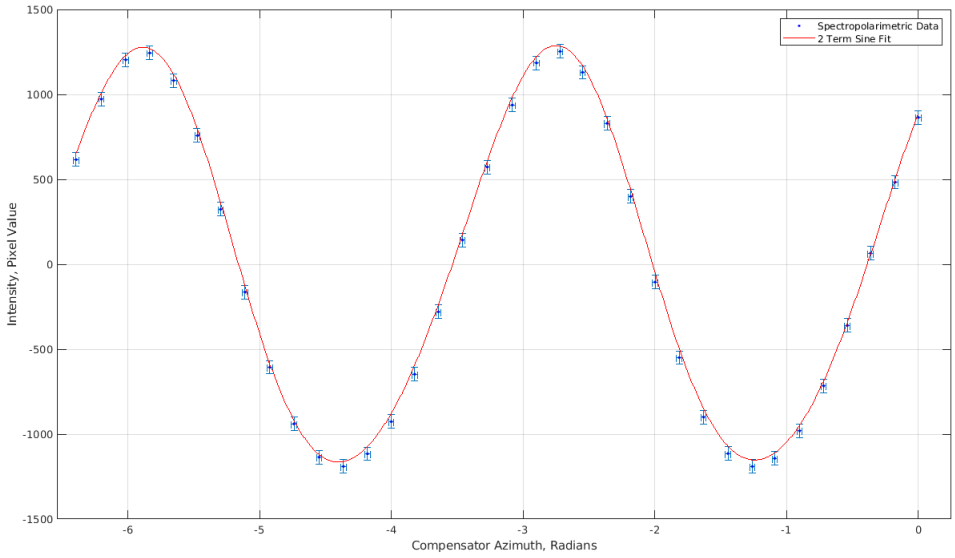

Figure 19: Two Term Sum of Sine Curve Fit, Circular Polarization Calibration, Horizontal Error Bars Scaled 10x

Curve fit results:

General model: a1*sin(b1*x+c1) + a2*sin(b2*x+c2) Coefficients (with 95% confidence bounds):

a1 = 1219 (1200, 1239); b1 = 1.997 (1.988, 2.005); c1 = 0.8355 (0.806, 0.8651);

a2 = -77.63 (-96.82, -58.44); b2 = 4.066 (3.932, 4.199); c2 = 2.877 (2.397, 3.358);

Average Intensity: 1.22×10^3

Adjusted R Squared = 0.9980, RMSE = 39.5016

Astronomical Data

Some data sets were acquired under the night sky. Objects observed included the Moon, Vega, and Arcturus. These data sets were collected with the 9.25" SCT and the spectropolarimeter at F/10. The lunar observation was made without the diffraction grating, therefore only polarimetric data was collected. This was done because of the comparatively large angular extent of the Moon, which would render any spectrum smeared and unusable. Polarimetric data were collected at 20^o intervals, with 1000 frames collected at each interval. These were analyzed in AutoStakkert!3 software, where the best 500 frames were selected and stacked. A ROI was selected and extracted from each stack. These frames can be seen in Figure 20. In MATLAB the average pixel intensity value was determined, and can be seen in the intensity plot in Figure 21. This was then fit with a sine curve, as seen in Figure 22, and a linearly decreasing sine curve as seen in Figure 23.

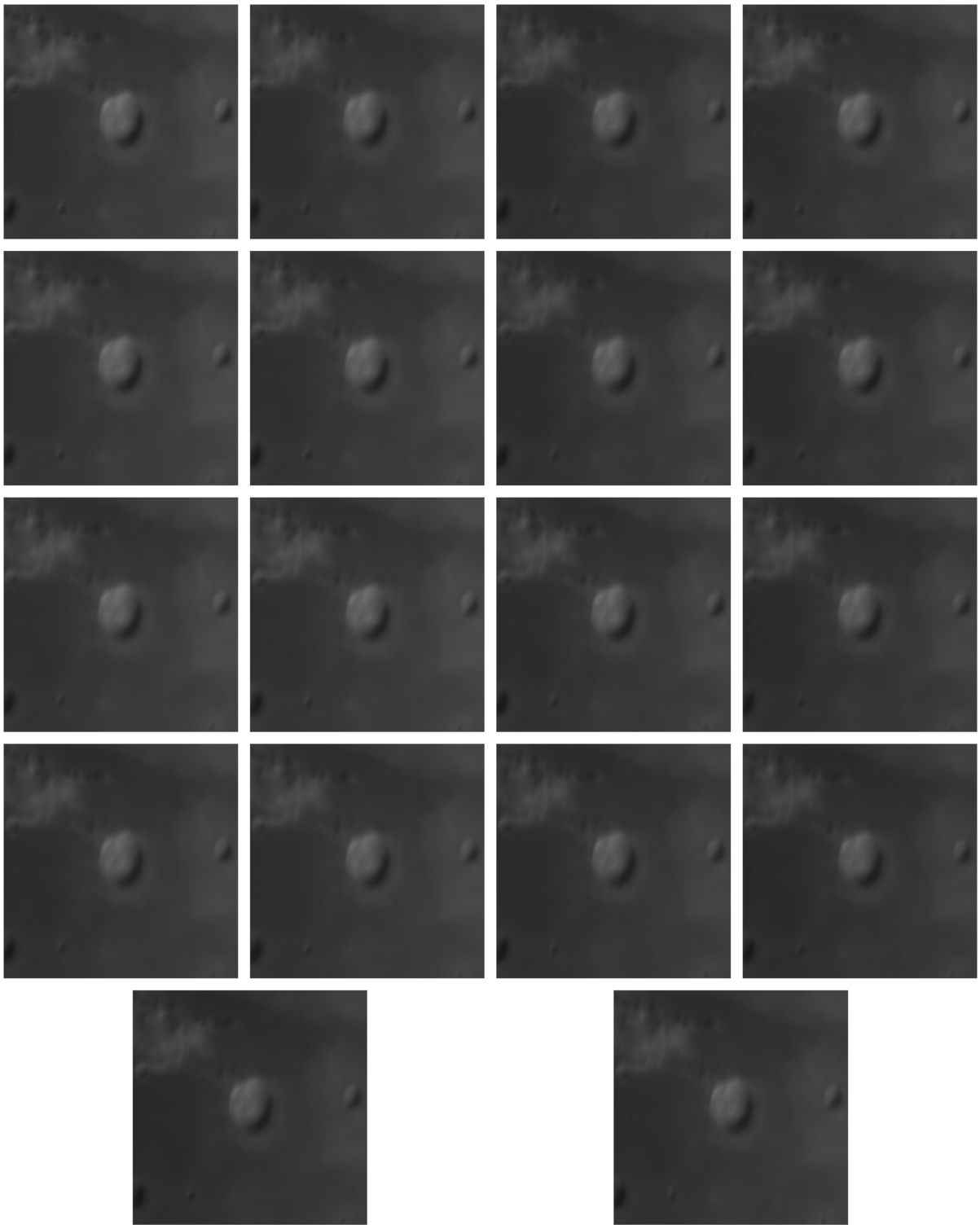

Figure 20: ROI frames Used in Lunar Polarimetric Measurement, 400x400 pixels

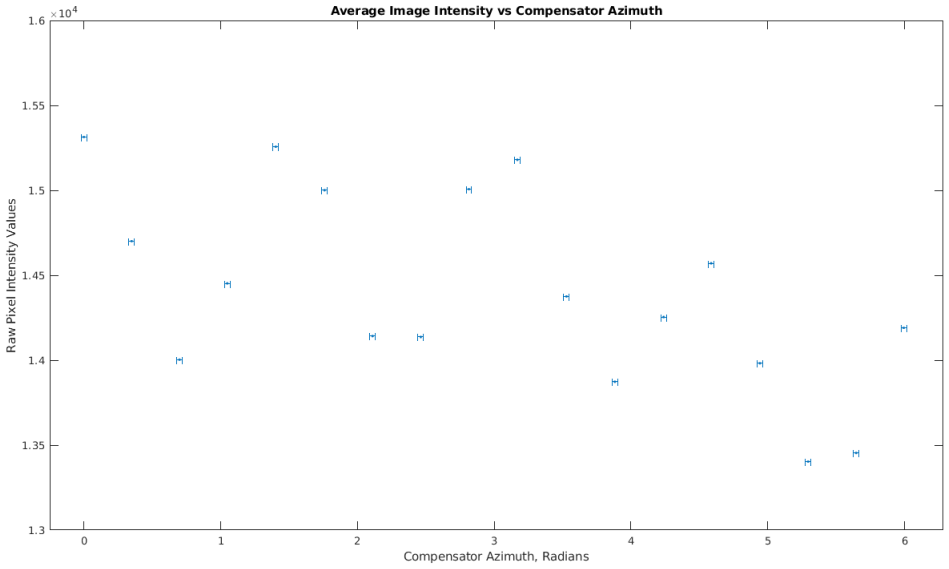

Figure 21: Lunar Polarimetric Intensity Plot, Horizontal Error Bars Scaled 10x

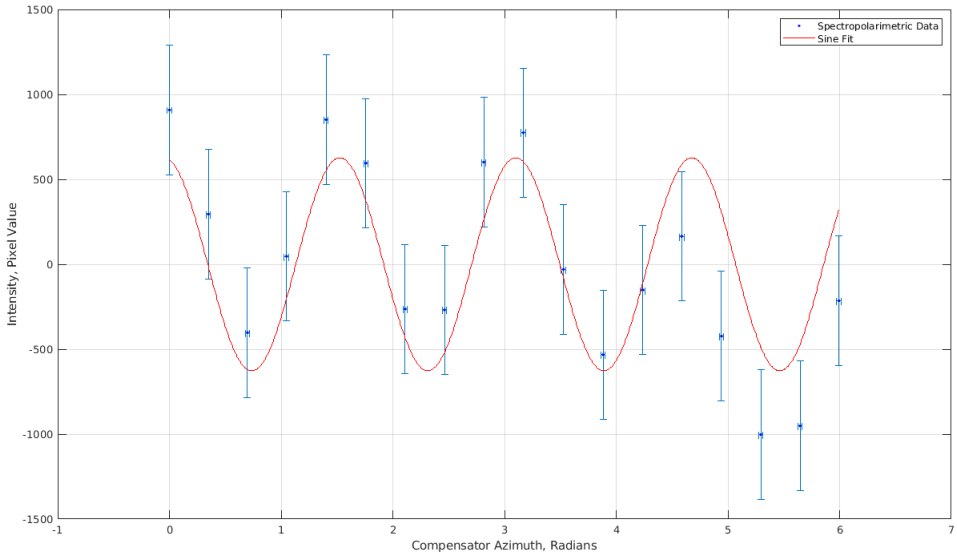

Figure 22: Lunar Intensity Plot, with Sine Curve Fit, Horizontal Error Bars Scaled 10x

Curve fit results: General model: a1*sin(b1*x+c1) Coefficients (with 95% confidence bounds):

a1 = 627 (356.3, 897.7); b1 = 3.988 (3.749, 4.227); c1 = 1.774 (0.911, 2.637);

Adjusted R Squared = 0.5696; RMSE = 380.8401

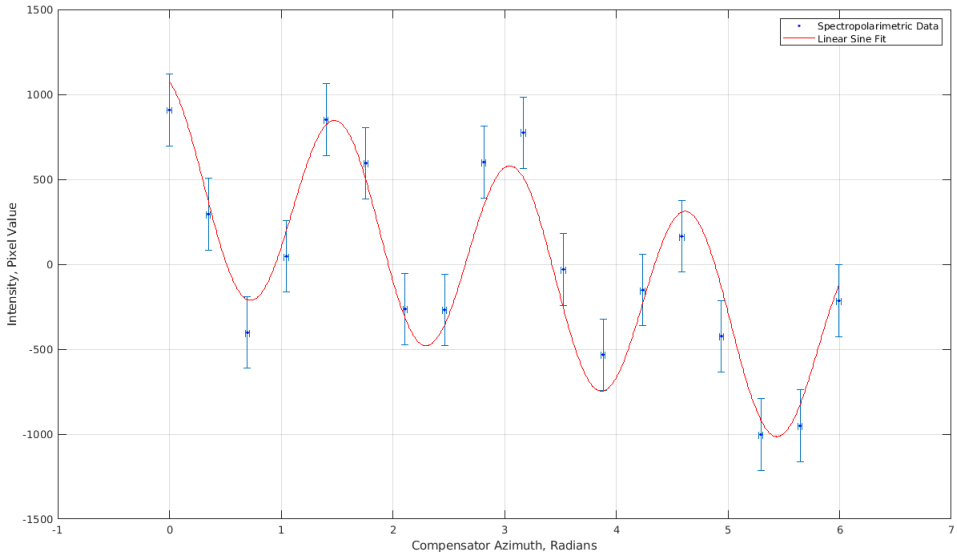

Figure 23: Lunar Intensity Plot, with Linear Sine Curve Fit, Horizontal Error Bars Scaled 10x

Curve fit results: General model: a1*sin(b1*x + c1) + d1*x + e1

Coefficients (with 95% confidence bounds):

a1 = 594.7 (442.8, 746.6); b1 = 4.001 (3.855, 4.147); c1 = 1.876 (1.356, 2.395);

d1 = -170.3 (-230.2, -110.3); e1 = 504.8 (294.8, 714.8);

Average Intensity = 1.4405×10^4;

Adjusted R Squared = 0.8991; RMSE = 210.8988

The diffraction grating was then reinserted into the instrument and a spectropolarimetric measurement was made on Vega. Data was collected at 20^o intervals, and around 10 frames were collected at each interval (exposures of 0.071s for Vega and 0.075s for Arcturus). These frames were analyzed with AutoStakkert!3 and the 5 best frames were selected and stacked. The ROI for each frame included the 0^{th} order image as well as the spectra in the frames. The raw intensity plot of the frames as a function of compensator azimuth angle can be see below in Figure 26, and the intensity plot with a two term sum of sine curve fit in Figure 27.

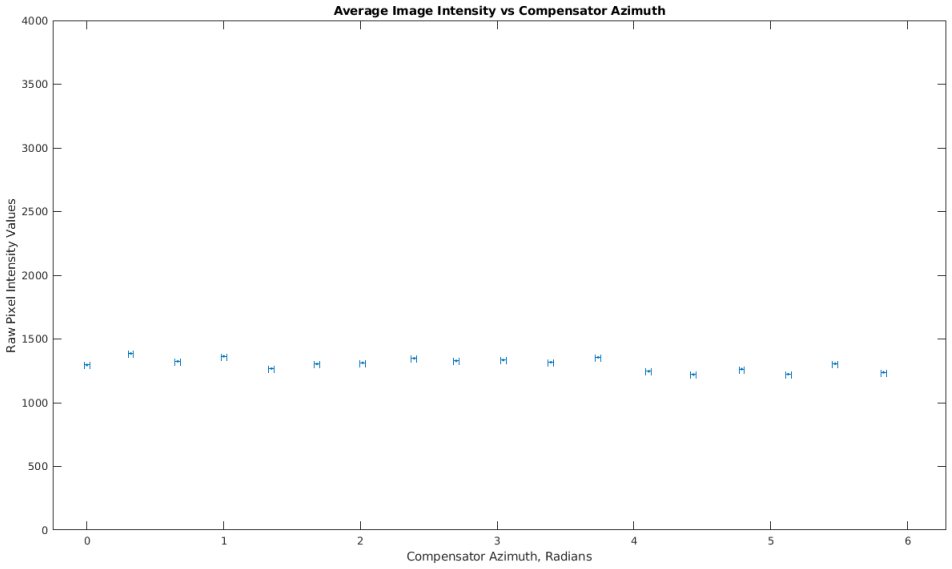

Figure 24: Polarimetric Intensity Plot, Arcturus, Horizontal Error Bars Scaled 10x

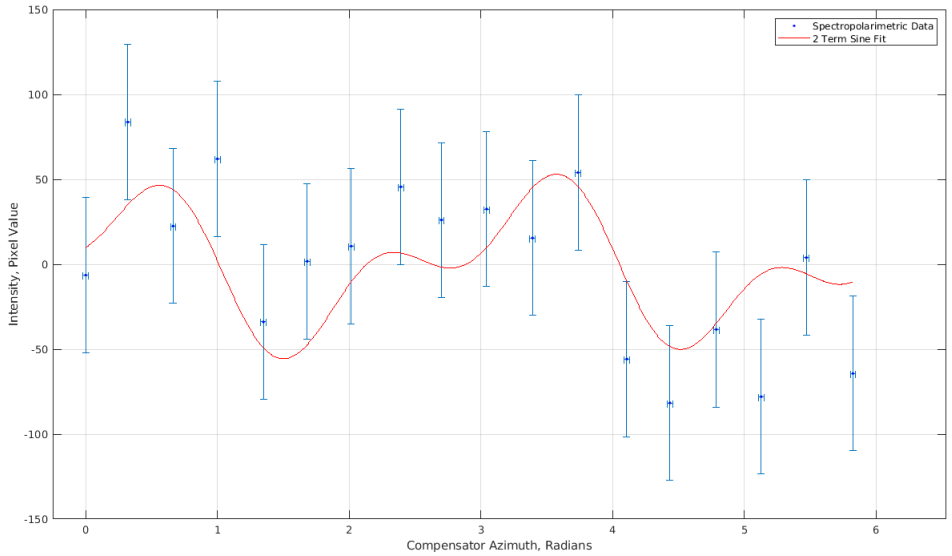

Figure 25: Polarimetric Intensity Plot, Arcturus, with Two Term Sum of Sine Curve Fit, Horizontal Error Bars Scaled 10x

General model Sin2: a1*sin(b1*x+c1) + a2*sin(b2*x+c2)

Coefficients (with 95% confidence bounds):

a1 = 35.63 (1.387, 69.88); b1 = 2.011 (1.455, 2.567); c1 = 1.238 (-0.7284, 3.205);

a2 = 24.76 (-8.284, 57.8); b2 = 4.215 (3.346, 5.084); c2 = -1.306 (-4.118, 1.507);

Adjusted R Squared = 0.1387; RMSE = 45.6343

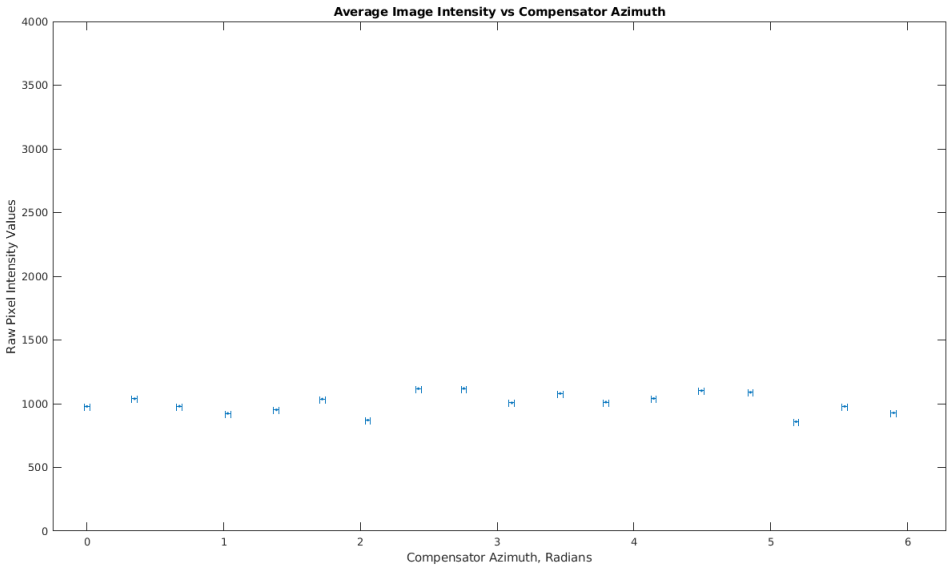

Figure 26: Polarimetric Intensity Plot, Vega, Horizontal Error Bars Scaled 10x

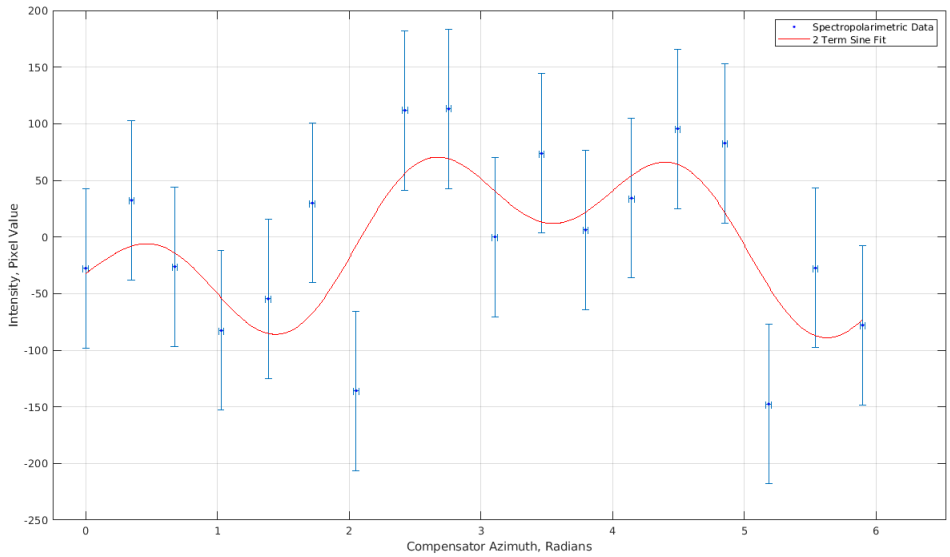

Figure 27: Polarimetric Intensity Plot, Vega, with Two Term Sum of Sine Curve Fit, Horizontal Error Bars Scaled 10x

Curve fit results: General model: a1*sin(b1*x+c1) + a2*sin(b2*x+c2)

Coefficients (with 95% confidence bounds):

a1 = 55.91 (4.887, 106.9); b1 = 1.204 (0.6269, 1.78); c1 = 3.64 (1.577, 5.703);

a2 = 43.96 (-9.415, 97.34); b2 = 3.141 (2.497, 3.786); c2 = -0.1224 (-2.394, 2.149);

Adjusted R Squared = 0.2206; RMSE = 70.4074

In the following spectral plots, the vertical columns of pixels in a single frame was averaged, and that average value plotted as a function of position on the sensor. Figure 28 shows a raw intensity plot, while Figure 29 shows a conversion to wavelength in nm, and finally 30 shows an adjusted wavelength conversion.

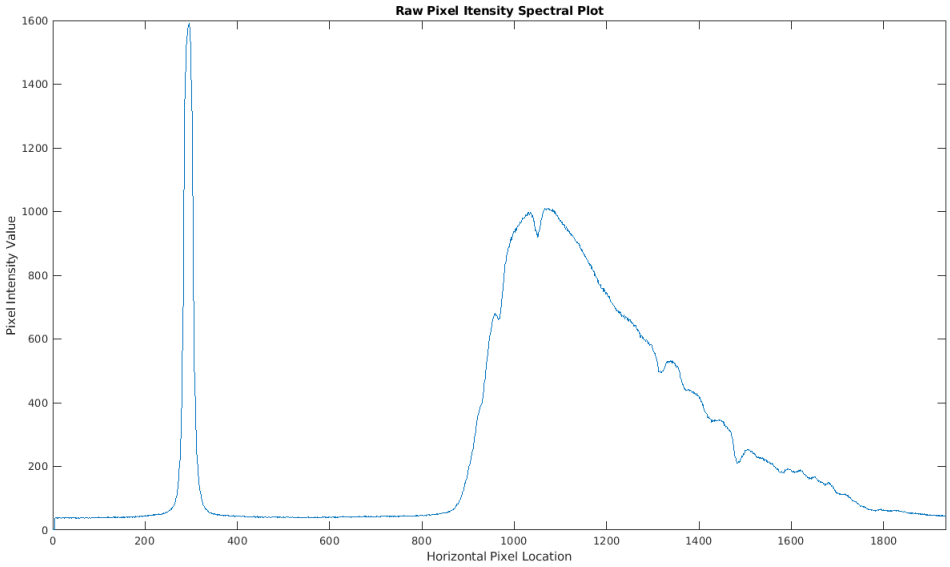

Figure 28: Raw Pixel Spectral Plot, Vega

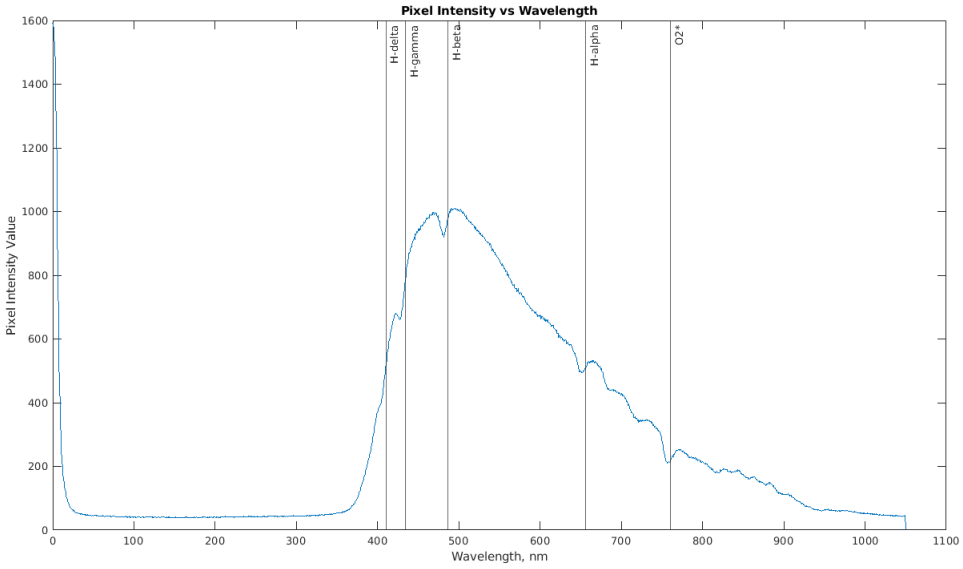

Figure 29: Spectral Plot, Vega, with Balmer Line Locations

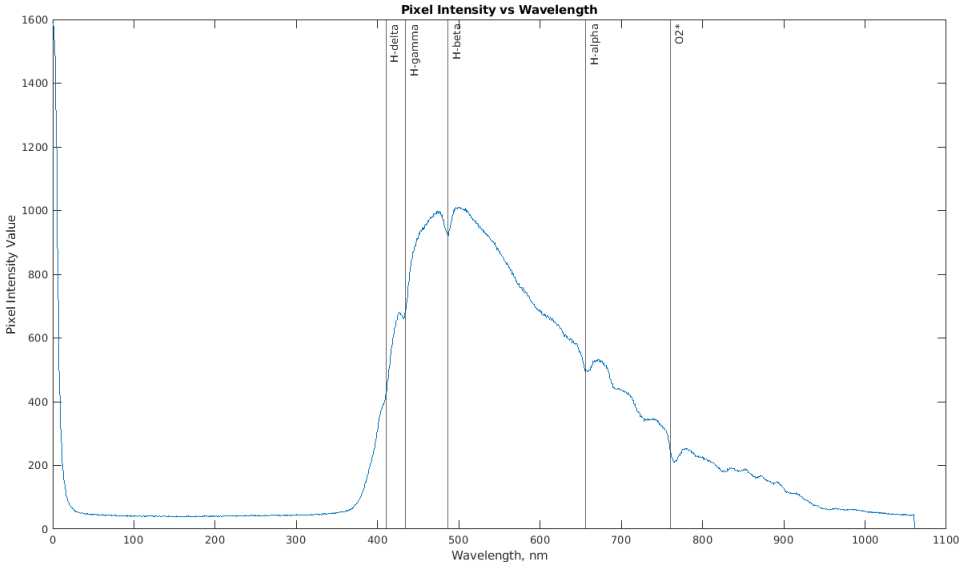

Figure 30: Adjusted Spectral Plot, Vega, with Balmer Line Locations
*OII line, compare to published data by Buil, [2]

For analysis, the intensity curves were inspected using MATLAB's curve fitting toolbox, essentially allowing a regression technique to determine the coefficients of Equation 18. Another form of analysis would be to use a Fourier analysis using the Fourier equations found in the Theory section, although it is not clear in this case that this form of analysis is better than the regression method used.

The linear polarization input plot seen in Figure 15 is similar to the theoretical output discussed in the Theory section and seen in Figure 2. To make use of MATLAB's curve fitting toolbox, the average value was subtracted to center the curve around zero. The results from the curve fit are an excellent fit to a 4^{th} harmonic signal, as would be expected from the input.

Similarly, the circularly polarized input produces an intensity plot seen in Figure 17 very similar to the expected theoretical result. Upon analysis with the curve fitting toolbox, a good fit was found using only a single sine term, as seen in Figure 18; however, it was discovered that an even better fit can be accomplished by allowing for two sine terms to be used as seen in Figure 19. Noting that the two frequencies that appear in the curve fit are 2θ and 4θ, it would be reasonable to conclude that there is some linear polarization component allowed through by the circular polarizer that was used.

Unfortunately, to conduct a full, proper analysis of the data, some knowledge of the analyzer azimuth and relative compensator azimuth angles is necessary. When the instrument was being assembled, the optics were inserted more or less indiscriminately with regard to orientation; in other words, the orientation of α in the equations described in the theory section is unknown. In the context of astronomical observation, knowledge of the analyzer azimuth is not strictly important (one could argue that the orientation in space is somewhat less meaningful and let α define the coordinate axis), but to complete analysis the relative angle between analyzer and compensator must be known. This could be determined by analyzing linearly polarized input light ϕ, given that the orientation of polarization in space is known. Unfortunately, while taking calibration data this was not recorded. Due to time constraints, this relation was not determined; however, so long as the instrument is not disassembled, the orientation of the optics relative to the potentiometer and each other should remain static, so this information can be gathered after the fact. Once this factor is determined, the Stokes parameters could be calculated according to Equations 23. This problem persists through the astronomical data collection.

This means for the data collected, there is ambiguity in the Stokes parameters S_1 and S_2, meaning

the orientation of the linear polarization (and azimuth of the major axis of elliptical polarizations) is ambiguous (See Equations 13). This ambiguity exists because there is a phase difference between the sine and cosine term that is not determined in Equation 18. However, with the data collected as is, even with ambiguity between S_1 and S_2, degrees of polarization can be determined, taking the amplitude of the 4θ frequency to be the magnitude of S_1 and S_2. For example, in the circular polarizer filter, it was noted that a two term sum of sine with 4θ and 2θ terms fit the data very well; using the amplitudes and comparing to Equation 18, it can be said that the degree of polarization in this filter is

$$\begin{aligned} \text{DOP} &= \frac{\sqrt{1219^2 + 77.63^2}}{1220} = 1.001 \\ \text{DOP}_{\text{circ}} &= \frac{1219}{1220} = 0.9992 \\ \text{DOP}_{\text{lin}} &= \frac{77.63}{1220} = 0.0636 \\ \chi &= \frac{609.5}{610 + 19.4075} = 0.968 \end{aligned}$$

Therefore, it can be said from this data that this filter produces perfectly polarized light (100.1%), with 99.92% circular polarization and 6.36% linear polarization. Note that these do not add perfectly. This may be due to non-ideal behaviors of the analyzer or other systematic errors that need to be accounted for.

While collecting astronomical data, one of the observations made about the instrument itself was the spectropolarimeter would not allow for proper focus at F/6.3. This is because the spectropolarimeter, as is, puts the camera sensor too far back, outside the range of focus travel of the telescope to use with a focal reducer. This problem can be mitigated by shortening the instrument. Two pieces in particular can be made shorter with no effect on the instrument: the adapter on the 72 tooth pulley as seen in Figure 6 could be reduced significantly, and the SCT to T-Mount adapter is unnecessarily long (shorter ones are sold). Combining these two factors, the author estimates that the instrument length could be at least be halved.

It should be noted that decreasing the focal length of the instrument does not change the linear dispersion on the sensor from the diffraction grating. The dispersion, as seen in Figure 5, is a function of the grating to sensor distance. Decreasing the focal length would have the advantage of increasing the intensity of light on the sensor, thus making a stronger signal, reducing the image size of the star on the sensor, which would increase spectral resolution, and decreasing the necessary tolerances on the telescope mounting to track precisely.

The lunar intensity plot seen in Figure 21 suggests a clear sinusoidal pattern. Upon analysis with the curve fitting toolbox, a 4θ signal is indeed reported. However, visual inspection of the intensity

plot suggests that the intensity of the plots overall decreases with time. It should be noted that for this plot, the angles were negated– this was done to emphasize the passage of time from left to right on the graph, instead of vice versa. In a proper polarimetric analysis these angles are the negative angle of the ones shown on the graph.

The linearly decreasing sine plot fits the data much better. The decrease of intensity with time might be attributed to the fact that the Moon was setting, and therefore its luminosity decreased with time as it became lower in the sky. The 4θ frequency reported from the curve fit indicates a linear polarization component to the signal. This is not entirely unexpected, as reflected light is preferentially polarized in the plane of reflection. This effect seems to be evident in the reflected Sunlight off of the Moon's surface. Doing a DOP analysis similar to that done on the circular polarizing filter:

$$\mathrm{DOP} = \mathrm{DOP}_{\mathrm{lin}} = \frac{594.7}{14405} = 0.0413$$

Therefore it can be said that linearly polarized light was detected in the analyzed moonlight with a degree of polarization of 4.13%. This value is in line with, but slightly lower than other measured values for degree of polarization in moonlight (lunar phase angle of 99°) [12], which might be attributed to the fact the ROI used here encompasses a crater near the lunar limb, not the terminator, which is more polarized.

A polarimetric analysis of starlight from both Arcturus and Vega, as seen in Figures 24, 25, 26, 27. Any detected polarization under this analysis seems uncertain at best. This is not entirely unexpected, as stars are not an objects that would be expected to polarize light. A curve fit procedure, similar to that done to the previous objects under analysis, seems to indicate the potential for 2θ and 4θ frequencies to be present in the signal. It should be noted that the moon was still present in the sky, and that these two objects were at significant angles in the sky away from the moon, meaning that scattered moonlight off of the atmosphere is likely to be polarized and may be present in the signal. To better determine if any polarization is present, a measurement should be made with no moon in the sky to add scattering polarization, more integration frames and/or longer integration times per frame could be used to decrease noise levels, and finally, more measurements at smaller angle intervals could be made to better determine frequency components.

Turning now to the spectral data, where the spectrum of Vega from one of the polarimetric frames was used. Vega was chosen because it is a type A0 star, which typically have very strong hydrogen absorption lines. These lines have a well known wavelength and can be used for calibration. The raw intensity plot as a function of horizontal position on the sensor is seen in Figure 28. This in

itself is not entirely informative; however this can be converted to a wavelength distribution using the computed number in Equation 9, and this result is seen in Figure 29.

It can be seen that absorption line dips in the spectrum nearly correspond to the location of the Balmer hydrogen lines. Using the H-α line, the plate scale was calculated and adjusted from the theoretical calculated value to be $0.6434\frac{\text{nm}}{\text{px}}$. This conversion was then used to plot the spectrum as a function of wavelength, as seen in Figure 30. It can be seen that across the Balmer lines, multiple absorption dips in the spectrum line up well, indicating a good fit.

FUTURE WORK

The spectropolarimeter constructed for this project shows much promise. On the instrument itself, more work is left in developing a more automatic routine for data collection. By better use of the data collection program using the ZWO ASI290mm SDK, an automatic data collection routine could be run on the Raspberry Pi. The spectropolarimeter currently uses a lot of back-focus distance, which prevents use at F/6.3 on a typical SCT. This could be fixed by shortening unnecessarily long components, such as the T-Mount adapter and the optomechanical rotation pulley to optical tube adapter.

Better characterization of the analyzer azimuth angle, or at least the relative angle between the analyzer and compensator, should be determined. Although this could be done with a careful note of how the linear polarizer is inserted into the instrument, and the ADC reading of the 0 angle noted, a better method would be to develop a calibration routine using various generated polarization states. The could account for any minor shifts or changes in the polarizer and quarter waveplate orientations in the optical tube, slight drifts in the potentiometer readings, and other variables.

The optical performance should be better analyzed to determine achromatic behavior of the components, especially the compensator, as waveplates are often not achromatic. The spectral performance needs better characterization, especially in terms of resolution and the limiting optical factors. For example, spectral resolution at this point is limited by the size of the image of the star on the sensor. Often resolution can be improved with the introduction of an entrance slit. Additionally, the off axis nature of the spectrum from a transmission grating means that optical aberrations impact resolution. Exploration into the use of a beam deviating prism in a "grism" arrangement could prove to be a positive impact on performance [13].

Reflection inherently effects polarization. The Schmidt-Cassegrain telescope design involves two mirrors to focus the light. The effects, if any, of these reflections should be accounted for. One possible procedure for this is to analyze generated polarized light directly through the spectropolarimeter without the telescope focusing the light, and analyzing that same generated light through the telescope. This would highlight any polarization effects of the optics in front of the spectropolarimeter.

The data gathered could be improved with longer integration times and more integration frames to reduce the noise in the image. More analysis into the limiting magnitude of this instrument should be made. For recording the angle of the quarter waveplate from the motor shaft, an optical encoder could be used, which would eliminate any restriction on the number of turns the shaft could make. Optical encoders are also not prone to changes due to temperature such as might be the case in a

potentiometer and the voltage source across it.

Determining under what circumstances a Fourier analysis is advantageous. It is suggested by Berry, Gabrielse, & Livingston that this form of analysis is especially well suited to fast, real time measurements where the analysis is done continuously to provide continuous polarization measurements, which is not an implementation well suited to this application.

Finally, the data collected does not take advantage of the full power of measuring the polarization of the spectrum. Future work could include the better collection and processing of data to analyze different parts of the spectrum in a polarimetric sense.

CONCLUSION

In conclusion, a theoretical description of a simple straight optical train, modulated signal based spectropolarimeter has been discussed. After light has been collected by a telescope, the optical design makes use of a rotating quarter waveplate (compensator), a fixed linear polarizer (analyzer), and transmission grating of $100l/\text{mm}$, with a ZWO ASI290mm astronomical camera acting as the sensor. The practical constraints on implementing such an instrument were discussed, and the construction of a spectropolarimeter was detailed, including the necessary optics, optomechanics, and electromechanics. The rotation and recording of the rotating compensator was facilitated by a motorized connection with proportional feedback control, and the uncertainty in measuring the angle was discussed. Calibration data of linear and circular polarizations was collected and analyzed, but full analysis of the light in terms of the 4 Stoke's parameters was hindered by lack of knowledge of the relative angle between analyzer and compensator, leading to ambiguity in the S_1 and S_2 parameters. However, this can be overcome by determining that relative angle with the correct calibration routine. Even with the ambiguity, degrees of polarization can be determined, and was applied to a circular polarization filter and lunar data. The analyzed moonlight exhibited clear linear polarization with a degree of polarization of 4.13%, while the polarimetric analysis of Vega and Arcturus suggested potential for polarization, but more analysis is needed, especially with the consideration of polarized reflected moonlight in the atmosphere. Spectroscopic performance was confirmed by measuring the hydrogen Balmer lines in Vega, leading to a plate scale of $0.6434\frac{\text{nm}}{\text{px}}$. In conclusion, a spectropolarimeter capable of measuring all 4 Stoke's parameters of stellar spectra collected with a telescope has been constructed and tested on known generated polarization signals and astronomical objects.

REFERENCES CITED

[1] P. Hauge and F. H. Dill, "A rotating-compensator fourier ellipsometer," *Optics Communications*, vol. Vol 14, Number 4, pp. 431–437, 1975.

[2] C. Buil, "Vega spectrum atlas." `http://www.astrosurf.com/buil/us/vatlas/vatlas.htm`, 2012-06. [Online; accessed 20-May-2020].

[3] "Basics of spectropolarimetry," *Proceedings of the International Astronomical Union*, vol. 9, no. S307.

[4] L. Wang and J. C. Wheeler, "Spectropolarimetry of supernovae," *Annual Review of Astronomy and Astrophysics*, vol. 46, p. 433–474, Sep 2008.

[5] D. J. Griffiths, *Introduction to Electrodynamics*. University Printing House, Cambridge CB2 8BS, United Kingdom: Cambridge University Press, 1989/2018.

[6] L. M. P. Frank L. Pedrotti and L. S. Pedrotti, *Introduction to Optics*. University Printing House, Cambridge CB2 8BS, United Kingdom: Cambridge University Press, 2018.

[7] G. G. H. G. Berry and A. E. Livingston, "Measurement of the stokes parameters of light," *Applied Optics*, vol. Vol 16, Number 12, pp. 3200–3205, 1977.

[8] C. U. Keller, "Astrophysical spectropolarimetry: Instrumentation for astrophysical spectropolarimetry," 2001.

[9] O. S. of America, *Handbook of Optics: Devices, measurements, and properties (Second Edition)*. McGraw-Hill, 1995.

[10] E. Collett, *Field Guide to Polarization*. P.O. Box 10 Bellingham, Washington 98227-0010 USA: SPIE—The International Society for Optical Engineering, 2005.

[11] Thorlabs, *PAX1000 Operation Manual*. Thorlabs.

[12] S. F. Pellicori, "Polarizing properties of pulverized materials with special reference to the lunar surface," *Appl. Opt.*, vol. 10, pp. 270–285, Feb.

[13] C. Buil, "A low cost spectrograph." `http://www.astrosurf.com/buil/us/spe1/spectro2.htm`, 2012-06. [Online; accessed 20-May-2020].

APPENDICES

```
#!/usr/bin/python3
##Jacob Marchio, University of Maine, 2020##
##Honors Thesis in Engineering Physics, Computer Engineering##
##"Design and Construction of a Computer Controlled Astronomical Spectropolarimeter"##
##The following is motor control code that reads an ADS1115ADC and
##uses an error proportional control to output a PWM signal to an H-Bridge.##
##Also records angle and error to a file##
import time
import board
import busio
import csv
import adafruit_ads1x15.ads1115 as ADS
import wiringpi
from numpy import sum, zeros, array
from adafruit_ads1x15.analog_in import AnalogIn
from adafruit_ads1x15.ads1x15 import Mode
from ctypes import *

i2c = busio.I2C(board.SCL, board.SDA)
wiringpi.wiringPiSetupGpio()
wiringpi.pinMode(12,1)
wiringpi.pinMode(17,1)
wiringpi.pinMode(27,1)
wiringpi.softPwmCreate(12,0,100)

ads = ADS.ADS1115(i2c)
chan = AnalogIn(ads, ADS.P0, ADS.P1)
ads.mode = Mode.CONTINUOUS
ads.gain = 1
RATE = 860 #128 #64 #250 #8 #475
ads.data_rate = RATE
```

```
data = zeros(10)
error = 20
iteration = 0
rec = open("rec.csv", "w")
writer = csv.writer(rec)

for i in range(10):
      data[i] = chan.value
      time.sleep(0.0012)

angle_zero = int(sum(data)10)
ep = 0
ang = 0
print("avg:  ", angle_zero)
print("err:  ", ep)
print("angle:  ", ang)
writestuff = []
writestuff.append(iteration)
writestuff.append(ep)
writestuff.append(angle_zero)
writestuff.append(ang)
writer.writerow(writestuff)

while(iteration!= 17):
      input()
      iteration += 1
      desired = chan.value + 522 #9396 = 360, 522 = 20, 261 = 10
      error = desired - chan.value
      dtycycl = 15
      kp = 0.3
      time.sleep(1)
```

```
      while(abs(error)!=0):
            error = desired - chan.value
#           print(error)
            if (abs(error)>250):
                  dtycycl = 75
            if (abs(error)<60):
                  dtycycl = 18
            else:
                  dtycycl = int(kp*abs(error))
            wiringpi.softPwmWrite(12,dtycycl)
            if (error < 0 ):
                  wiringpi.digitalWrite(17,0)
                  wiringpi.digitalWrite(27,1)
            if (error > 0 ):
                  wiringpi.digitalWrite(17,1)
                  wiringpi.digitalWrite(27,0)

            wiringpi.digitalWrite(17,0)
            wiringpi.digitalWrite(27,0)

      for i in range(10):
            data[i] = chan.value
            time.sleep(0.0012)
      avg = int(sum(data)10)
      ep = desired - avg
      ang = float(angle_zero - avg)26.1
      print("avg:  ", avg)
      print("err:  ", ep)
      print("angle:  ", ang)

      writestuff = []
      writestuff.append(iteration)
      writestuff.append(ep)
```

```
        writestuff.append(avg)
        writestuff.append(ang)
        writer = csv.writer(rec)
        writer.writerow(writestuff)

rec.close()
```

```
 %%Jacob Marchio, University of Maine, 2020%%
%%Honors Thesis in Engineering Physics, Computer Engineering%%
%%"Design and Construction of a Computer Controlled Astronomical Spectropolarimeter"%%
%%Image Processing Code%%
%%The following reads a sequence of images and motor CSV data file%%
%%and pulls polarimetric and/or spectroscopic data from frames%%
%%expects frame filenames to be sequentially numbered%%

% Get a list of all files in the folder with the desired file name pattern.
filePattern = fullfile('.specpolmoonframes', '*.tif'); %reads all tif files in directory
theFiles = dir(filePattern);

%reads CSV file containing motor data.  Expects:  iteration,error(digital values),
%location(digital value),location(angle)
motordata = csvread('.specpolmoonmoon_rec.csv');

for k = 1 :  length(theFiles)
      baseFileName = theFiles(k).name;
      fullFileName = fullfile('.specpolmoonframes', baseFileName);
      fprintf(1, 'Now reading %s\n', fullFileName);
      imageArray = imread(fullFileName);

      %reduce vertical ROI (depends on subject)
      %imageArray = imageArray(180:225,:); %white led
      %imageArray = imageArray(597:643,:); %green led
      %imageArray = imageArray(385:430,:); %blue led
      %imageArray = imageArray(835:880,:); %red led
      %imageArray = imrotate(imageArray, -0.7, 'bilinear');

      %reduce horizontal ROI if desired (depends on subject)
      spec = imageArray;
      %spec = imageArray(:,1250:1500);
```

```
M = mean(spec); %vector of mean of vertical columns
y = linspace(1,length(M),length(M));
[fpath,fname,ext] = fileparts(baseFileName);
data(k).name = str2num(fname); %name of the frame, should be a number
data(k).data = imageArray; %image data
data(k).avgI = mean2(spec); %average intensity of whole frame

%name for spectrum plot
%specname = strcat('.specpolarbpolblue',fname,'spec.tiff');
imshow(spec);
%imwrite(spec,specname,'tiff');
%spectrum plot details
%{
plot((y*0.6366)- 187.797,M);
title("Pixel Intensity vs Wavelength")
xlabel("Wavelength, nm")
ylabel("Pixel Intensity Value")
xline(656.3,'-','H-alpha')
xline(410.2,'-','H-delta')
xline(434.0,'-','H-gamma')
xline(486.1,'-','H-beta')
xline(760.5,'-','O2*')
ylim([0 1600])
xlim([0 1100])
%}
%{
plot(y,M);
ylim([0 1600])
xlim([0 1936])
title("Raw Pixel Itensity Spectral Plot")
xlabel("Horizontal Pixel Location")
ylabel("Pixel Intensity Value")
%}
```

```
     drawnow; % Force display to update immediately.
end
%convert struct to cell to reshape and order by frame number
datafields = fieldnames(data);
datacell = struct2cell(data);
sz = size(datacell);

datacell = reshape(datacell, sz(1), []);
datacell = datacell';
datacell = sortrows(datacell, 1);
datacell(:,4) = num2cell(motordata(:,4));

x = linspace(0,2*pi);

angles = cell2mat(datacell(:,4))*pi/180;
intensities = cell2mat(datacell(:,3));
avgint = mean2(intensities);
OffsetIntensity = intensities - avgint;
errorbar(angles, intensities, 0.02*ones(size(angles)), '.', 'horizontal');
xlim([-0.25 2*pi])
%xlim([(-2*pi)-0.25 0.25])
ylim([13000 16000])
title('Average Image Intensity vs Compensator Azimuth')
xlabel('Compensator Azimuth, Radians')
ylabel('Raw Pixel Intensity Values')

%saveas(gcf, ".specpolmoonint.png");

%choose which curve fit to use:  sine, 2 term sum of sine, linearly
%decreasing sine, or 2 term linearly decreasing sum of sine
%[sinfitresult, singof]=sinfit(angles, OffsetIntensity)
%[sum2sinfitresult,sum2singof]=sum2sin(angles, OffsetIntensity)
[sinlinfitresult, sinlingof] = sinlin(angles, OffsetIntensity)
```

```
%[sumsinlinfitresult, sumsinlingof] = sumsinlin(angles, OffsetIntensity)



function [fitresult, gof] = sinfit(angles, normedint)
%CREATEFIT(ANGLES,NORMEDINT)
% Create a fit.
%
% Data for 'untitled fit 1' fit:
% X Input :  angles
% Y Output:  normedint
% Output:
% fitresult :  a fit object representing the fit.
% gof :  structure with goodness-of fit info.
%
% See also FIT, CFIT, SFIT.

% Auto-generated by MATLAB on 10-May-2020 18:12:44


%% Fit:  'untitled fit 1'.
[xData, yData]| = prepareCurveData( angles, normedint );

% Set up fittype and options.
ft = fittype( 'sin1' );
opts = fitoptions( 'Method', 'NonlinearLeastSquares' );
opts.Display = 'Off';
opts.Lower = [-Inf 0 -Inf];
opts.StartPoint = [773.690369576358 2 1.44375887798107];

% Fit model to data.
[fitresult, gof] = fit( xData, yData, ft, opts );
```

```
% Plot fit with data.
figure( 'Name', 'Sine Fit' );
%h = plot( fitresult, xData, yData );
errorbar(xData, yData, (gof.rmse)*ones(size(yData)), (gof.rmse)*ones(size(yData)), 0.02*ones(size
0.02*ones(size(xData)), '.');
hold on
xlim([-0.25 (2*pi)+0.25])
%xlim([(-2*pi)-0.25 0.25])
h = plot( fitresult, xData, yData );
legend( h, 'Spectropolarimetric Data', 'Sine Fit', 'Location', 'NorthEast' );
%text(0,min(yData)-20,sprintf('Adjusted R-Squared of Fit:%g',gof.adjrsquare))
% Label axes
xlabel('Compensator Azimuth, Radians')
ylabel ('Intensity, Pixel Value')
grid on
```

APPENDIX 2: COMMENTS ON EXTENDING TO THE EMERA ASTRONOMY CENTER

In brainstorming ideas for this project, one idea that was discussed was that of a spectroscopic instrument for use on the EMERA 20" CDK telescope. The following is some commentary on potential for extension of functionality of this spectropolarimeter for use with that optic.

Instrumentation on the CDK becomes, ideally, somewhat permanent fixtures, not needing to be attached and detached each time. This means that in order to maintain the current functionality of the telescope, a light path deviating flip-mirror would be necessary to switch the light path from the current instrumentation to the new instrumentation or vice versa. A different option would be to have an off-axis prism (outside the light path of the current sensor) sending light directly to the spectropolarimeter. Either way, the unnecessary length of the current spectropolarimeter would need to be addressed to allow for proper focus.

Before adding a spectropolarimeter to the EMERA 20" CDK, it should be ensured that spectropolarimter can take full advantage of the 20", F/6.8 telescope. Considerations, for example, should include whether vignetting from the 1" optics in the spectropolarimeter decrease the aperture. Additionally, an exploration into the use of collimating optics in the spectropolarimeter to collimate the F/6.8 light cone should be completed to determine by how much data quality is improved by by eliminating angular dependence in the quarter waveplate, polarizer, and diffraction grating. Highest quality optics would be desirable, for example, exchanging the polymer quarter waveplate for a true quartz achromatic plate. Given the high focal length and resolution possible from a 20" telescope, improvements made possible by an entrance slit for spectroscopy should be determined, as well as the use of higher ruling density diffraction gratings and a prism in a "grism" arrangement.

The automatic data collection program would need to be completed, and the programming run from the current computers running the other telescope instrumentation. The precision and freedom of rotation afforded by an optical encoder on the motor shaft would prove advantageous. Finally, an effective calibration routine for use within the observatory would need to be developed to fully determine the orientation of polarized light measured.

AUTHOR'S BIOGRAPHY

Jacob was raised in Beauregard, Alabama, where rural country land and dark skies by night fed his curiosity and desire to learn. Homeschooled from a young age all the way through high school, he was able to structure his studies to focus on his interests in science but especially astronomy and physics. He spent hours using telescopes and reading on optics and photography and spent his spare time in photography, astronomy, and astrophotography. In 2012 he submitted and was awarded a Highly Commended place in the international Astronomy Photographer of the Year Competition (Under 16 Category) by the Royal Observatory Greenwich, and the following year (2013) was awarded First Place and a Highly Commended place in the same category. He carried his love for astronomy and science into higher education with his major of Engineering Physics (Computer Engineering Concentration) in 2016, becoming part of the UMaine Class of 2020. During his undergraduate education, he worked at the EMERA Astronomy Center as an educator and telescope operator, using the university's 8" Alvan Clark telescope for public shows each week. He also worked for the Advanced Structures and Composites Center, and spent two of his three summers doing research at Auburn University in Auburn, Alabama.